ISTANBUL TECHNICAL UNIVERSITY★EURASIA INSTITUTE OF EARTH SCIENCES

PETROGENESIS OF THE SARICAKAYA INTRUSIVE ROCKS (ESKIŞEHIR, NW TURKEY) AND THEIR IMPLICATIONS

M.Sc. THESIS

Malik OTHMAN

Climate and Marine Sciences

Earth System Sciences

DECEMBER 2016

ISTANBUL TECHNICAL UNIVERSITY★EURASIA INSTITUTE OF EARTH SCIENCES

PETROGENESIS OF THE SARICAKAYA INTRUSIVE ROCKS (ESKIŞEHIR, NW TURKEY) AND THEIR IMPLICATIONS

M.Sc. THESIS

Malik OTHMAN
(601141010)

Climate and Marine Sciences

Earth System Sciences

Thesis Advisor: Prof. Dr. Gültekin TOPUZ

DECEMBER 2016

İSTANBUL TEKNİK ÜNİVERSİTESİ★AVRASYA YER BILIMLERI ENSTITÜSÜ

SARICAKAYA SOKULUM KAYALARININ (ESKİŞEHİR, KB TÜRKİYE) PETROJENEZİ VE ÖNEMLERİ

YÜKSEK LİSANS TEZİ

Malik OTHMAN
(601141010)

Iklim ve Deniz Bilimleri

Yer Sistem Bilimleri

Tez Danışmanı: Prof. Dr. Gültekin TOPUZ

ARALIK 2016

Malik Othman, a M.Sc. student of ITU Eurasia Institute of Earth sciences, student ID 601141010 successfully defended the thesis/dissertation entitled "PETROGENESIS OF THE SARICAKAYA INTRUSIVE ROCKS (ESKIŞEHIR, NW TURKEY) AND THEIR IMPLICATIONS", which he prepared after fulfilling the requirements specified in the associated legislations, before the jury whose signatures are below.

Thesis Advisor:	**Prof. Dr. Gültekin TOPUZ** ISTANBUL Technical University	.....
Jury Members:	**Prof. Dr. Aral OKAY** ISTANBUL Technical University	.....
	Prof. Dr. Osman CANDAN Dokuz Eylül University	.....

Date of Submission: **25 November 2016**
Date of Defense: **19 December 2016**

To my dear parents,

FOREWORD

I am deeply grateful to my supervisor Prof. Dr. Gültekin Topuz for his guidance in preparing this thesis, and for his technical, financial and personal support.

This study is partly supported from the scientific research unit of the İstanbul Technical University. Without this funding, field work and part of the analytical works would not have been possible.

Thin section preparation by Mahir Altınbağa is highly appreciated.

Parts of the preliminary drafts of the thesis were read by Gönenç Göçmengil. I am thankful for his careful reading and suggestions for the modification.

Finally, I would like to thank my friends, Mohammed Kabiru, Sefa Şahin, Amr Nasser and Alisurat Guliyev for their support during my study.

December 2016 Malik OTHMAN

TABLE OF CONTENTS

ABBREVIATIONS

ACS	: American Chemical Society
ASI	: Aluminum Saturation Index
cm	: centimeter
cn	: Chondrite-normalized
HFSE	: High field strength elements
HNO_3	: Nitric acid
HREE	: Heavy rare earth elements
Hz	: Hertz
ICP	: Inductively Coupled Plasma
I-type	: Igneous-type
km	: kilometer
LA	: Laser ablation
$LiBO_2$	: Lithium metaborate
LILE	: large ion lithophile elements
LOI	: Loss on ignition
LREE	: Light rare earth elements
Ma	: Mega-annum
MC	: Multi collector
MEVD	: Multi-element variation diagrams
min	: Minute
ml	: Milileter
mm	: Millimeter
MS	: Mass spectrometer
MTA	: Maden Tetkik ve Arama
N	: North
NW	: Northwest
pmn	: Primitive mantle normalized
ppm	: Part per million
REE	: Rare earth elements
S	: South
S-type	: Sedimentary-type
TAS	: Total alkali versus silica
wt	: Weight

LIST OF TABLES

Page

LIST OF FIGURES

Page

LIST OF SYMBOLS

~	: About
≥	: Greater than or equal
µ	: Micron
%	: Percent

PETROGENESIS OF THE SARICAKAYA INTRUSIVE ROCKS (ESKIŞEHIR, NW TURKEY) AND THEIR IMPLICATIONS

SUMMARY

This work deals with petrogenesis of the granitic rocks within the Sarıcakaya complex in western part of Sakarya zone. The Sarıcakaya complex is unconformably overlain by Middle Jurassic limestone and locally by Early Jurassic clastic rocks to the north, and is thrust over Late Triassic greenschist-facies metabasite and marbles (the Karakaya Complex). In addition, the Sarıcakaya complex is covered by the Tertiary continental sedimentary rocks to the southeast. In this study we employed deferent methods include geological mapping, sampling, petrographic description and bulk rock geochemical analysis.

The metamorphic rocks are represented by amphibolite-facies micaschist, gneiss, amphibolite and metagranite. These rock assemblage is characteristic of a continental crust rather than a former oceanic accretionary complex. The metamorphic rocks are crosscut by (i) quartz diorite, (ii) biotite granite, (iii) mafic-ultramafic cumulate stocks, and (iv) voluminously minor felsic granites represented by two-mica granites and leucogranite with local muscovite and garnet. The contact metamorphic effects are only obvious around the gabbro-peridotite cumulate complexes. These mafic-ultramafic cumulate rocks are formerly erroneously regarded as part of an ophiolite.

The quartz diorite is metaluminous and medium to high-potassium calcalkaline I-type signature. It has probably formed as a consequence of substantial mantle involvement. Besides the cumulate rocks formed primarily by accumulation processes of a mantle-derived basic magma. The hornblende-biotite granite is peraluminous and I-type granite with high-potassium alkaline nature. The leucogranite and two-mica granites are strongly peraluminous S-type granites, and represent partial melting products of continental crust. Available geochronological data on intrusive rocks from the literature suggest that the plutonism in the Sarıcakaya Complex occurred during Early to Late Carboniferous. Regional geological constrains are consistent with magmatic arc to post-collisional setting.

SARICAKAYA SOKULUM KAYALARININ (ESKİŞEHİR, KB TÜRKİYE) PETROJENEZİ VE ÖNEMLERİ

ÖZET

Bu çalışmanın konusu Sakarya Zonu'nun batısında yer alan Sarıcakya Kompleksi içerisindeki granitik kayaların petrojenezini kapsamaktadır. Bu çalışma amacı Sarıcakaya plutonik kayaçlarının petrojenezini incelemeyi amaçlar. Bu çalışmada jeolojik haritalam, petrografi ve tüm kaya jeokimyası yöntemleri kullanılmıştır. Sarıcakaya bölgesinde yer alan sokulum kayalar, Sakarya Zonu'nun (Pontidler, Kuzey Türkiye) Jura öncesi temelinin bir parçasıdır. Sonuç olarak, Sarıcakaya sokulum kayaçalarının petrojenezinin anlaşılması, Sakarya bölgesinin Jura öncesi evrimini sınırlamaya yardımcı olacaktır.

Sakarya bölgesi ağırlıklı uyumsuz heterojen bir temele sahip olup, bu temelin üzerine Jura ve genç tortul ve volkanik kayalar gelmektedir. Sakarya bölgesinin Jura öncesi temel kayaları (örneğin Artvin, Pulur ve Gümüşhane (Doğu Sakarya bölgesi), Yenişehir ve Sarıcakaya (Orta Pontidler) görülür.

Bu çalışmada, jeolojik haritalama, örnekleme, petrografik tanımlama ve toplam kaya jeokimyasal analizi gibi farklı yöntemle kullanılmıştır.

Arazi çalışmaları sırasında 160 km2'lik bir alada gerçekleştirilmiştir. Farklı kaya türleri arasındaki sınır ilişkileri ortaya çıkarılmıştır. Metamorfik ve plutonik kayaçlar da dahil olmak üzere yaklaşık 220 temsilci numune toplanmıştır. Arazi çalışmalarından sonra, seçilen örneklerden 60 ince bölüm hazırlanmış ve petrografik olarak tanımlanmıştır. Tüm kayaç analizi, çalışma alanı boyunca farklı kaya türlerinden 35 örnek üzerinde yürütülmüştür.

Sarıcakaya Kompleksi Orta Jura yaşlı kireçtaşları ve yersel olarak Erken Jura yaşlı klastik kayalar tarafından uyumsuzlukla örtülmekte, ayrıca Geç Triyas yeşilşist fasiyesli metabazit ve mermerleri (Karakaya Kompleksi)'nin üzerine bindirmektedir. Bunun yanı sıra, Sarıcakaya Kompleksi, güneybatı kesiminde Tersiyer karasal sedimanları tarafından örtülmektedir.

Metamorfik kayalar amfibolit fasiyesindeki mikaşist, gnays, amfibolit ve metagranit ile temsil edilemektedir. Metamorfik kayaçlar migmatitik gnays, mikaşist, amfibolit ve küçük metagranit ve metagabro ile temsil edilmektedir. Genellikle iyi gelişmiş yapraklanma gösterirler. Gnayslar lökosomlar ve melanozomlar tarafından tanımlanan migmatitik dokular sergilerler. Amfibolitte 0.5-10 cm kalınlıkta yaprak-paralel felsik damarlar vardır. Bu damarlar yersel olarak yaprak dokusu gösterir. Metagranitlerde yapraklanma gösterir ve porfiritik dokulara sahiptir. Uzunlamasına büyümüş K-feldispat'lar karakteristiktir.

Bu kaya topluluğu okyanusal bir yığışım karmaşasından ziyade, kıtasal kabuk karakteristiği göstermektedir. Metamorfik kayalar (i) kuvars diyorit (ii) biyotit granit (iii) mafik-ultramafik kümülat stoklar ve (iv) hacimsel olarak ufak, iki mikalı granit ve muskovit-granatlı lökogranitlerden oluşan felsik granitler tarafından kesilmektedir.

Kontak başkalaşımının izleri sadece gabro-peridotiti kümülat komplekslerinin olduğu alanlarda gözlenmektedir. Söz konusu mafik-ultramafik kümülat kayaları önceki çalışmalarda hatalı bir biçimde bir ofiyolit parçaları olarak değerlendirilmiştir.

Kuvars diyorit, doğu-batı yönünde, yaklaşık 20 km uzunluğunda ve ~ 3 km uzunluğunda bir yüzlek oluşturur ve böylece çalışma alanındaki en büyük kütleye sahiptir. Genel olarak aşırı deform ve altere bir şekildedir. Arazide genel olarak koyu renkli-yeşilimsi-gri renkler sunmakta, bunun yanı sıra minerallerin tane boyutu orta ila kaba (0.5-5.1 mm) arasında değişmektedir. Kuvars diyorit ağırlıklı olarak masiftir. Bununla birlikte, bazı yerlerde zayıf bir yapraklanma görülmektedir. 10 cm kalınlığa kadar ulaşan mafik mikrogranüler anklavlarda içermektedir.

Kuvars diyorit, plajiyoklas, amfibol, biyotit, kuvars ve opak mineral (ilmenit)lerden oluşmaktadır. Bunun yanı sıra, apatit, zirkon gibi yardımcı fazlarda içerir. İkincil mineraller serisit (beyaz mika) ve klorittir. Bu ikincil mineraller sırasıyla biyotit ve plajiyoklası ornatmaıktadır. Lokal olarak yüzleklerde kuvars miktarı artmaktadır, bu nedenle kuvars diyorit tonalite doğru geçiş gösterir. Amfibol ve biyotit minerallerinde de opaklaşma vardır

Hornblend-biyotit granit, farklı üç gövde halinde, ve uzamış şekillerde gözlenir. En büyük yüzlekleri, 10 km uzunluğunda ve 2 km boyunca uzanmaktadır. Kaya türü, pembe ila açık gri renkte ve orta taneli (1-3 mm) boyutları belirgindir. Masif doku yaygın olarak gözlenir. Bu birim genel olarak eş tane boylu olup, plajiyoklas, K-feldispat, kuvars, biyotit ve amfibol mineralleri içerir. Opak mineral, apatit ve zirkon aksesuar minerallerdir. Serisit ve klorit ise ikincil minerallerdir.

Lökogranit, inceleme alanı boyunca, metamorfik kayaçlara küçük stoklar (~ 800 m çapında) dayk / oyuklar (1 ila 50 m kalınlık) şeklinde yerleşmiştir. Lökogranitler genel olarak masiftir. Bazı kesimlerind grafik doku sergilemektedir. Tane boyutları üniform değildir ve aplitikten pegmatite kadar değişmektedir (1 mm'den 2 cm'ye). Granat ve muskovit yersel olarak görülür. Lökogranit genel olarak ortoklaz, plajiyoklas, kuvars ve küçük granat ve muskovit minerallerinden oluşmaktadır.

İki mikalı granit, çalışma alanının kuzey bölümündeki (yaklaşık 0,8 km uzunluğunda ve 0,5 km boyunca) metamorfik kayaçlar içinde ufak bir stok oluşturmaktadır. Koyu gri bir renkli olup ve orta ila küçük taneli taneler (0.2-2 mm) gösterir. Kaya genel olarak masifdir, ancak zayıf bir yapraklanmada sergilemetedir. Granat-muskovitli kesim, nispeten daha eştane boyulu bir dağılım göstermektedir. Başlıca kuvars, plajiyoklas, muskovit, biyotit ve K-feldispattan (ortoklaz ve mikroklin) oluşmaktadır.

Kümülat gabro ve peridotit kompleksi, metamorfik kayaçlardaki çeşitli yerlerde küçük stoklar (3 km'ye kadar en büyüğü) şeklinde bulunur. Koyu gri ila siyah renkte, ince ila orta dereceli tane boylarına sahiptir (1-2 mm. Bazı kesimlerde hafifçe serpantinite dönüşme vardır. Sokulumun etrafında, belirgin bir kontakt metamorfik halesi geliştirilmiştir. Kompleks genel olarak peridotit ve gabrodan oluşur.

Kuvars diyorit, dar bir jeokimyasal aralıkta yer almaktadır. (SiO_2 = 59-63 wt%, Al_2O_3 = 17 – 18 wt%, FeO* = 5.20 – 6.28 wt%, MgO = 2.63 – 3.52 wt%, Na_2O = 2.5 – 3 wt%, K_2O = 1.8 – 2.8 wt%). Kuvars diyorit, petrografik incelemelerle uyumlu olarak, K2O + Na2O ve Si02 diyagramında diorite alanına izdüşmektedir. Alüminyum doygunluk indeksi (ASI) 0.95'den 1.05'e kadar değişir. Yüksek ASİ değerleri, muhtemelen serisit ve klorit gibi ikincil minerallerin oluşumu ile ilgilidir. Magnezyum numarası (Mg #) 46.5 'den 50 'ye kadar değişir. Kuvars diyoritin hornblend içermesi

alüminyum içeriğiyle tutarlıdır. Bileşik çeşitliliğin dar olmasına rağmen, Al_2O_3, Fe_2O_3tot, MgO, CaO, Sr ve Y oranları artan SiO_2 ile azalır.

Biyotit-hornblend granitler aşırı alterasyonu maruz kalmıştır. Bu nedenle sadece bir adet örnekten jeokimyasal analiz yapılmıştır. Bu numune (SiO_2 = 74.96 wt%, Al_2O_3 = 13.46 wt%, FeO* = 0.98 wt%, MgO = 0.1wt%, Na_2O = 3.63 wt%, K_2O = 3.76 wt%) bileşim ile karakterize edilmiştir. Biyotit-hornblend granit K2O + Na2O'ya karşı SiO2 (TAS) diyagramında granit alanına izdüşmektedir. Bu durum petrografik incelemeler ile uyum göstermektedir.

Alüminyum satürasyon indeksi (ASI) ve Mg sayısı sırasıyla 1.13 ve 15.36'dır. Bu durum kayanın peralüminsus karakterli oldğunu gösterir. Peccerillo & Taylor'dan (1976) SiO2-K2O diyagramında ise numune yüksek-K kalk-alkalin alana düşer.

Lökogranit, toplam K2O + Na2O'ya karşı SiO2 (TAS) diyagramında granit alanında, yer almaktadır ve orta-yüksek K kalk-alkalin serisine kadar geniş bir potasyum aralığında saçılmaktadır (K_2O = 1.94 – 4.08 wt%; Na_2O =3.27 – 5.41 wt%). Benzer şekilde, P_2O_5 içerikleri büyük ölçüde değişir (0.05 to 0.20 wt%). Bununla birlikte diğer ana oksitler daha dar bir değişim göstermektedir (SiO_2 = 74.22 – 76.80 wt%, Al_2O_3 = 13.82 – 15.02 wt%, FeO* = 0.27 – 1.54 wt%, MgO = 0.04 – 0.08 wt%). K_2O ve Na_2O içeriğindeki büyük değişimler, normal granitik ve pegmatitik bölgelerde yapılan örnekleme ve mineralerin tane boyularındaki büyük farklılıkalrla açıklanabilir. Alüminyum satürasyon indeksi (ASI), peralüminus kökeni gösteren 1,16 ila 1,35 arasında değişmektedir.

Kuvars diyorit metalüminus karakterli, orta ve yüksek K'lı, kalk-alkalen, I tipi izler sergilemektedir. Birim olasılıkla önemli miktarda manto etkisi ile oluşmuştur. Bunun yanı sıra kümület kayaları, manto kökenli bazik bir magmanın birikmesi ile oluşmuştur. Hornblend-biyotit granitler ise peralüminus, I tipi ve yüksek potasyumlu alkalin karakter sergiler. Lökogranit ve iki mikalı granitlerde baskın olarak peralüminus S tipi karakter göstermekte olup, kıtasal kabuğun kısmi ergimesi ile oluşmuşlardır. Literatürde söz konusu kayalar için bilinmekte olan jeokronolojik veriler, Sarıcakaya Kompleksi içerisindeki plütonizmanın Erken-Geç Karbonifer yaşlı olduğunu göstermektedir. Kuvars diyorit magmatik yay ortamında oluşma olasılığı yüksektir. Bunun aksine, iki mika graniti muhtemelen kıtasal kabuğun kısmi ergimesinden dolayı çarpışma ile eş zamanlı/sonra oluşmuştur. Kabuğun erimesi, Variskan orojenezinde (Sakarya zonu ile Laurasia kıtası arasındaki çarpışma) sıkışma ile açıklanabilir. Bu durum olasılıkla kabuk kalınlaşmasına, yükselmeye ve kalın kabuğun erimesine neden olmuştur. Bölgesel jeolojik gözlemler, magmatizmanın, magmatik yay ve çarpışma ortamında oluşumu destekler niteliktedir.

1. INTRODUCTION

Granitic rocks are essential component of continental crust. They are found in various geotectonic settings such as magmatic arcs, continental-collision zones and anorogenic intraplate settings (e.g. Bonin, 1988; 2007; Bonin et al., 2002; Bonin and Bébien, 2005; Wedepohl, 1991). They form either by fractionation from a mafic magma or from partial melting of crustal rocks as seen in high-grade metamorphic terranes. Sources of the granitic rocks can be sedimentary (metapelitic to metapsammitic) rocks (S-type granites), or igneous rocks ranging in composition from basic to acidic rocks (I-type granites). Their evolution and source are traced through geochemistry. Hence, they are important for the understanding the evolution of the continents over geological times.

1.1 Purpose and Scope

The purpose of this study is to constrain the petrogenesis of the Sarıcakaya plutonic rocks (Eskişehir, NW Turkey) by field geology, petrography and whole rock geochemistry. The Sarıcakaya intrusive rocks are part of the pre-Jurassic basement of the Sakarya Zone (Pontides, northern Turkey). Consequently, the understanding of the petrogenesis of the Sarıcakaya intrusive rocks will help to constrain the pre-Jurassic evolution of the Sakarya zone. Within the framework of this thesis I studied the intrusive rocks in the Sarıcakaya complex (Figure 1.3).

1.2 Geological Frame of Turkey

Turkey is located on the Alpine-Himalayan mountain range (Tethyan realm), and consists of several continental fragments between the Ukrainian shield (Laurasia) in the north and Arabian platform (Gondwana) in the south (Figure 1.1). These continental blocks are the Pontides (made up of the Strandja, Istanbul and Sakarya zones), the Antolide-Tauride block, the Kırşehir massif and the Arabian platform. These continental blocks are separated by sutures representing traces of the closed oceanic domains. The main ones are İzmir-Ankara-Erzincan suture (IAES) and Bitlis-Zagros suture (BZ). These oceans were mainly consumed by north-vergent subduction. During the course of elimination of Tethyan ocean, these continental blocks

amalgamated into a single landmass during the Tertiary (Ketin, 1966; Şengör and Yılmaz, 1981; Okay and Tüysüz, 1999; Okay 2008).

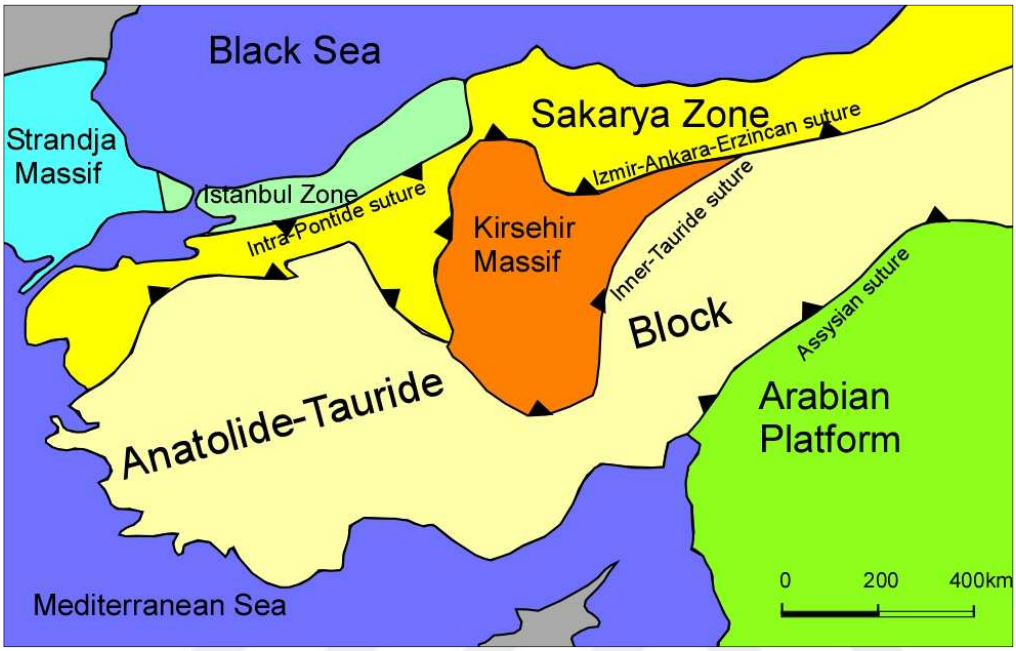

Figure 1.1: Major tectonic units of Turkey separated by suture zones (modified after Okay and Tuysuz, 1999).

1.3 The Sakarya Zone

The Sakarya zone is an east-west trending continental block, ~1500 km long and ~120 km across (Figure 1.1). It is bound by the Antolide –Tauride block and Kırşehir massif to the south, and Istanbul and Strandja zones to the north (Şengör and Yılmaz, 1981; Okay and Tüysüz, 1999). The boundaries are defined by Izmir-Ankara-Erzincan and Intra-Pontide sutures.

The Sakarya zone is mainly made up of Jurassic and younger sedimentary and igneous rocks which unconformably sit on a heterogeneous basement of pre-Jurassic age (Okay et al., 2006). The Jurassic and Late Cretaceous igneous activity is related to north-vergent subduction of the northern branch of the Neo-Tethys along Izmir-Ankara-Erzincan suture (Şengör and Yılmaz, 1981; Okay et al., 2006).

The pre-Jurassic basement of the Sakarya zone is exposed in several places (e.g. Artvin, Pulur and Gümüşhane (Eastern Sakarya zone), Yenişehir and Sarıcakaya (Central Pontides)) and can be broadly divided into four distinct rock associations. These are (i) amphibolite- to granulite-facies metamorphic rocks of Early

Carboniferous age (330-310 Ma) (Okay, 1996; Topuz et al., 2004, 2007; Okay et al., 2006). (ii) high-K I-type granitoids with Devonian, Carboniferous or Permian crystallization ages as reported by Delaloye and Bingöl (2000); Topuz et al (2010); Dokuz (2011); Ustaömer et al (2012); Kaygusuz et al (2012, 2016); Aysal et al (2012) and minor S-type (two-mica) granitoids of Permian age (Nzegge, et al 2006). (iii) Late Carboniferous to Early Permian sedimentary rocks, Okay and Leven (1996), and (iv) low grade metamorphic complexes (the Karakaya complex), consisting of Permo-Triassic metabasites, marble, and phyllite, interpreted as an accretionary complex (Okay and Göncüoğlu, 2004; Okay et al, 2002; Topuz et al, 2004b, 2014). Figure 2.2 shows the distribution of these basement units in the Sakarya Zone.

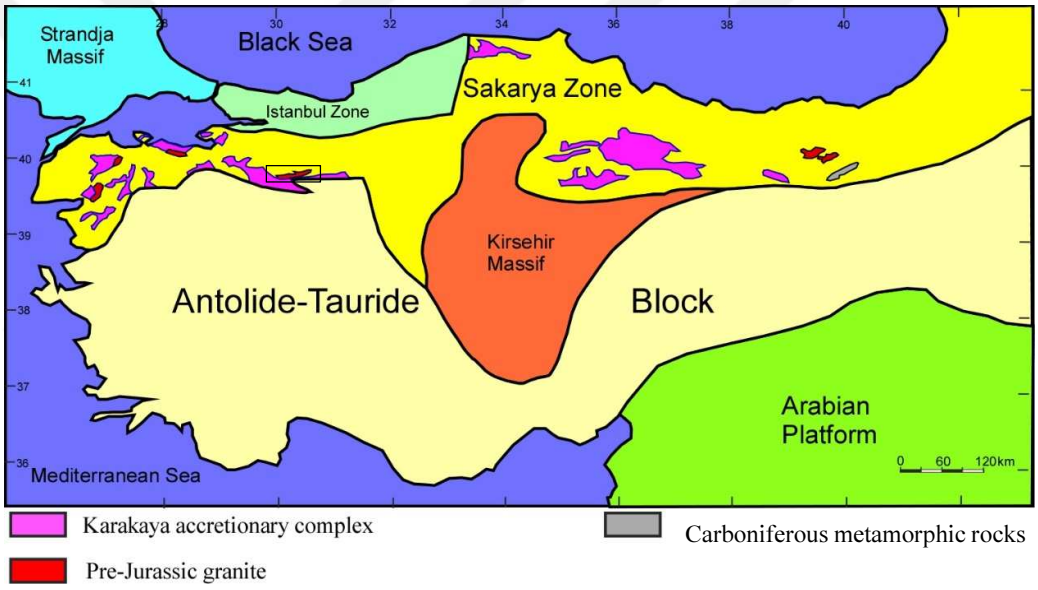

Figure 1.2: Distribution of the basement outcrop and the location of the Sarıcakaya complex in the Sakarya zone (modified after Okay, 2008).

1.4 The Sarıcakaya Complex

The Sarıcakaya complex is located in the western part of the Sakarya zone to the north of Izmir-Ankara- Erzincan suture zone (Figure 1.1, 1.3). This east-west trending complex, ~60 km long and ~8 km across, is located north of the historical city "Söğüt" and extents eastward to the area north of Sarıcakaya town and cut by the Sakarya river near to İnhisar (Figure 1.3).

The complex is made up of metamorphic and intrusive rocks (Yılmaz, 1977; Kadıoğlu et al, 1994; Göncüoğlu et al, 1996, 2000; Ustaömer et al, 2012; İlbeyli et al, 2015). It is bound locally by Early Jurassic clastic rocks (Bayırköy formation) and mainly by

Middle Jurassic limestone (Bilecik limestone) to the north. To the south, it is thrust over the Triassic Karakaya accretionary complex which is made up of Late Triassic marble, metabasites and phyllite. To the southeast part, it is unconformably covered by the Tertiary continental sedimentary rocks (the Mihalgazi formation) (Figure 1.3).

The region has subjected of several geological studies dealing with petrology, geochemistry and tectonic sittings. Available radiometric dating has been carried out only intrusive granitoids. K-Ar and Ar-Ar mica and hornblende ages as well as U-Pb zircon ages range from early Carboniferous to early Permian (327 to 270 Ma) (e.g. Çoğulu et al., 1965; Çoğulu and Krumennascher, 1967; Okay et al., 2002; Ustaömer et al., 2012). The metamorphic rocks are not dated. Based on these ages the metamorphics should be either older than Carboniferous or as Carboniferous. The mafic-ultramafic plutonic rocks are regarded part of an ophiolite by Göncüoğlu et al (2000). On the basis of geochemistry, the granite magmatism was ascribed either to arc magmatism as reported by Yılmaz (1977); Göncüoğlu et al (2000); Kibici et al (2010); Ilbeyli et al (2015), or to post-collisional setting (Kadıoğlu et al., 1994).

This postgraduate thesis deals with the geochemistry of the middle part of the Sarıcakaya complex (Figure 1.3).

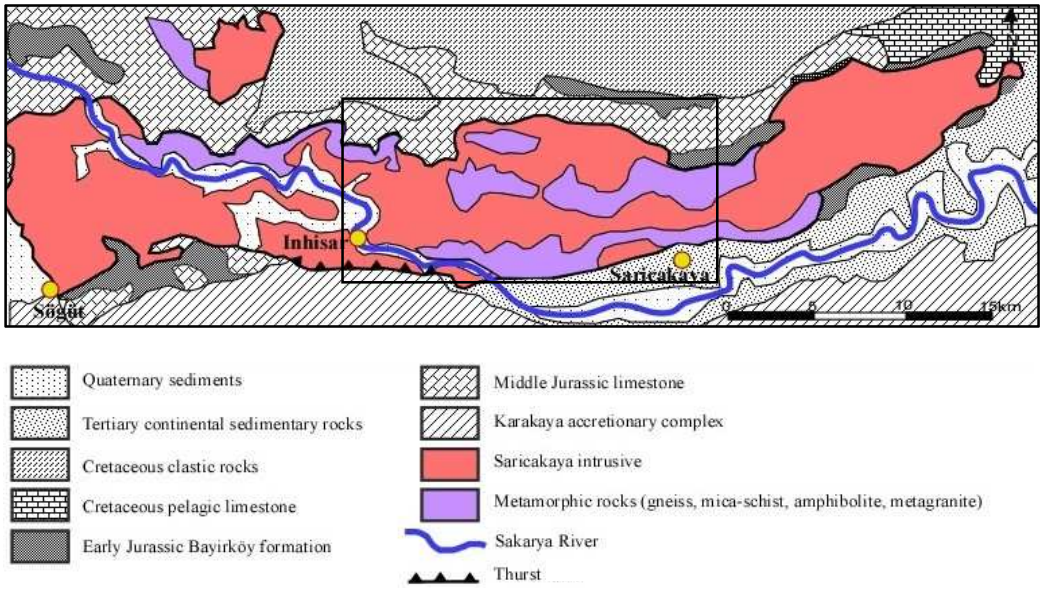

Figure 1.3: Generalized map of the Sarıcakaya complex and surrounded rocks, and location of the study area (modified after General directorate of mineral research and exploration (MTA, 2003/4, Turkey)).

1.5 Methods of Study

Methods employed in this study include geological mapping, sampling, petrographic description and bulk rock geochemical analysis. During the field work, an area of 160 km2 was mapped. Field relations between different rock types were established. Around 220 representative samples were collected, including metamorphic and plutonic rocks. Following field work, 60 thin sections from the selected samples were prepared and petrographically described. Whole rock analyses were carried out on 35 samples of different rock types across the study area.

Powdering the samples for whole rock analyses were performed at sample preparation laboratories of the Eurasian Institute of Earth Sciences (Istanbul Technical University). Major and trace element analysis were done at Acme Analytical Laboratories Ltd. in Vancouver, Canada. 200 mg of rock powder were mixed with 1.5 g of $LiBO_2$ flux in a graphite crucible. Subsequently, the crucible was placed in an oven and heated to 1050°C for 15 min. The molten samples were dissolved in 5 % HNO_3 (ACS grade nitric acid diluted in demineralized water). International reference samples and reagent blanks were added to the sample sequence. For analyses of major elements and the trace elements Ba, Nb, Ni, Sr, Sc, Y and Zr, sample solutions were aspirated into an ICP emission spectrograph (Jarrel Ash AtomComb 975). For the determination of other trace elements including rare earth elements, the solutions were aspirated into an ICP mass spectrometer (Perkin-Elmer Elan 6000). Accuracy for major elements is better than 2 % and for trace elements better than 10 % relative.

2. FIELD RELATIONS AND PETROGRAPHY

In this chapter, field relations of the Sarıcakaya metamorphic and intrusive rocks together with petrography are described separately.

2.1. The Sarıcakaya Complex

The studied part of the Sarıcakaya complex, ~20 km long and ~8 km across, consists of high grade metamorphic rocks and different types of intrusions (Figure 2.1). The complex is bound unconformable locally by early Jurassic clastic rocks (the Bayırköy formation) and mainly by the Middle Jurassic limestone (the Bilecik limestone) to the north. (Figures 1.2, 2.1 and 2.2). To the south, it is thrust over Triassic Karakaya accretionary complex (Figures 2.2). Tertiary continental sedimentary rocks unconformably cover the complex to the southeast (Figure 2.1).

The metamorphic rocks include amphibolite-facies migmatitic gneiss, micaschist, amphibolite, and minor metagranite and metagabbro (Figures 2.4, 2.5, 2.6 and 2.7). The intrusive rocks are represented mainly by quartz diorite and hornblende-biotite granite, subordinately by muscovite-garnet pegmatitic granite (leucogranite), two-mica granite, and cumulate gabbro-peridotite complex. Contact metamorphism is mostly not obvious around quartz diorite and hornblende-biotite granite. It is only marked around the cumulate gabbro-peridotite stocks.

Below field features of the metamorphic and intrusive rocks are described separately.

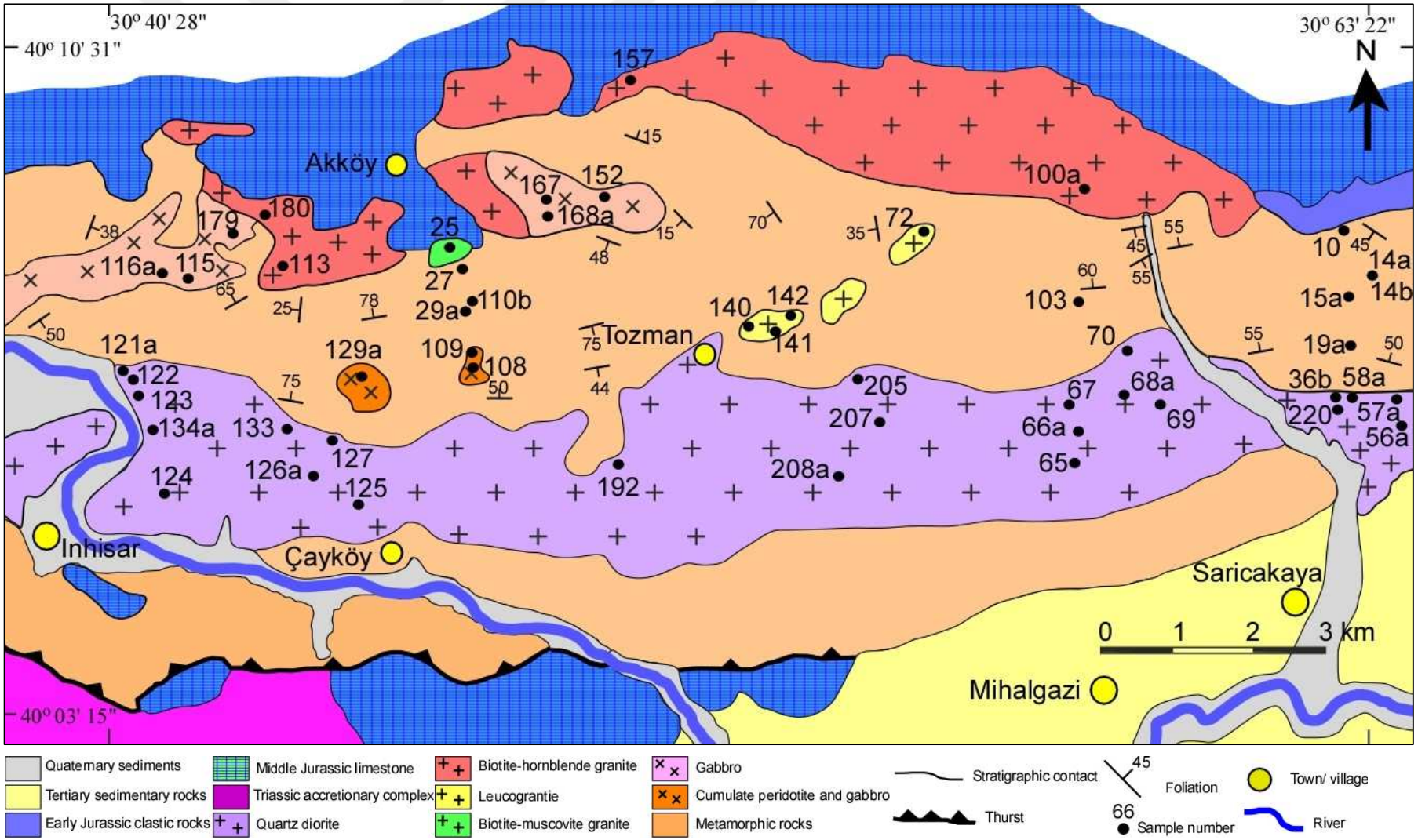

Figure 2.1: Geological map of the study area, Central Sarıcakaya complex.

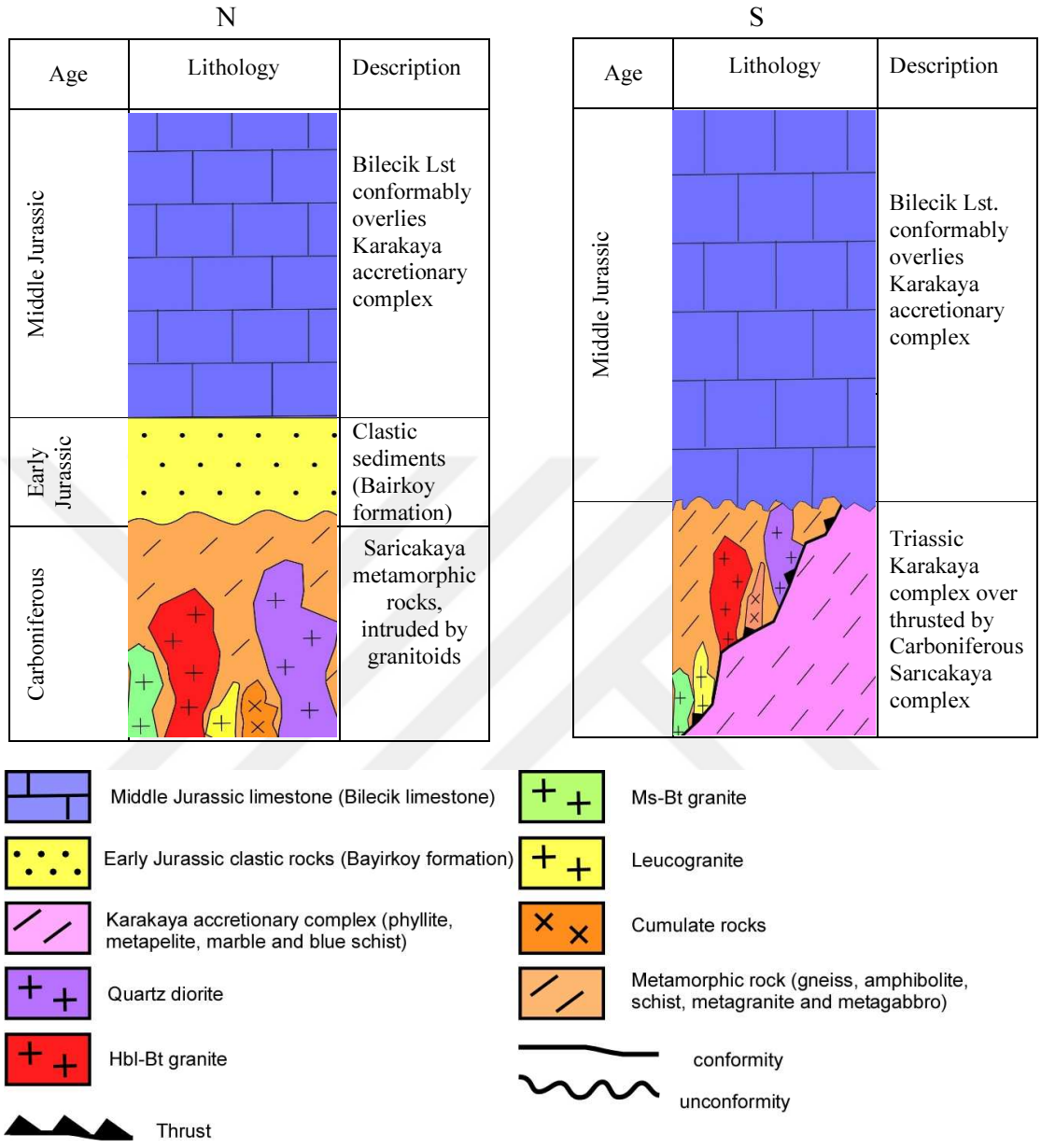

Figure 2.2: Geological columnar section of the study area.

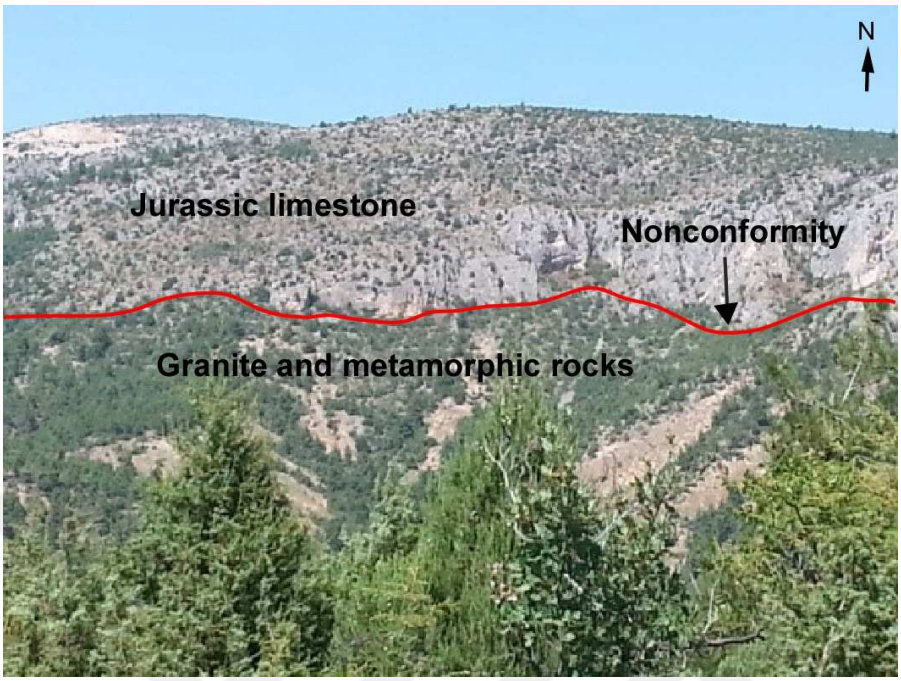

Figure 2.3: Middle Jurassic limestone (Bilecik limestone) (~3 km west of Akköy village) nonconformably overlies granitic and metamorphic rocks of the Sarıcakaya complex.

Figure 2.4: Early Jurassic clastic sedimentary rocks of the Bayırköy formation (conglomerate, sandstone and shale) locally unconformably overlies the metamorphic and granitic rocks.

2.2. The Sarıcakaya Metamorphic Rocks

The metamorphic rocks are represented by migmatitic gneiss, micaschist, amphibolite and minor metagranite and metagabbro. They generally display well-developed foliation (Figure 2.5). The gneisses displays migmatitic fabric defined by leucosomes and melanosomes (Figure 2.6). In amphibolite there are 0.5 to 10 cm thick foliation-parallel felsic veins. These veins locally crosscut the foliation (Figure 2.7). The metagranite is foliated and forms porphyritic texture. It shows large, elongated crystals of K-feldspar (Figure 2.8).

Figure 2.5: Well-developed foliation in the high-grade metamorphic rocks of the Sarıcakaya complex (~2.6 km northeast of Çayköy village)

Figure 2.6: Leucosomes and melanosomes in migmatitic gneiss (~4 km north of Sarıcakaya town, Sarıcakaya complex). Diameter of the coin is 26 mm.

Figure 2.7: Felsic veins (0.5 – 10 cm) in the amphibolite. Felsic veins are parallel to the foliation and locally cross-cut it (~1.3 km east of the Çayköy village, the Sarıcakaya complex).

Figure 2.8: Well foliated metagranite with K-feldspar (~ 1.7 km west of Tozman village, Sarıcakaya complex).

The migmatitic gneisses are fine grained (0.01-0.3 mm), and consist of biotite, plagioclase, K-feldspar, quartz and sillimanite (Figure 2.9). The sillimanite forms fibrous crystals (fibrolite) (Figure 2.9), and occurs locally as inclusion in plagioclase and quartz.

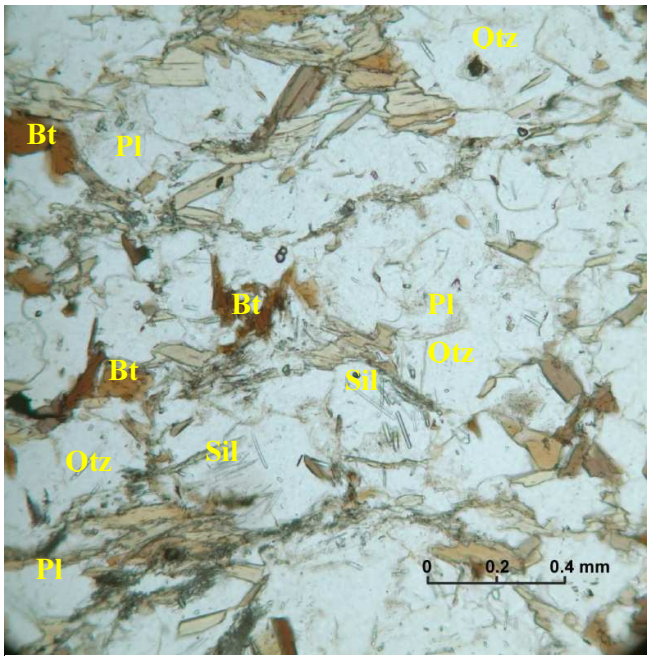

Figure 2.9: Sillimanite-biotite gneiss, Sarıcakaya complex (~2 km south east of Akköy village). Qtz: Quartz, Ms: Muscovite, Bt: Biotite, Pl: Plagioclase, Sil: Sillimanite.

Micaschists are well-foliated, fine to medium grained (0.25-1.2 mm). They made up of quartz, plagioclase, biotite and muscovite (Figure 2.10). Quartz grains are generally anhedral, and show undulatory extinction. Biotite is common and form elongated crystals. Minor minerals are zircon, apatite, and opaque minerals as rounded inclusions in quartz.

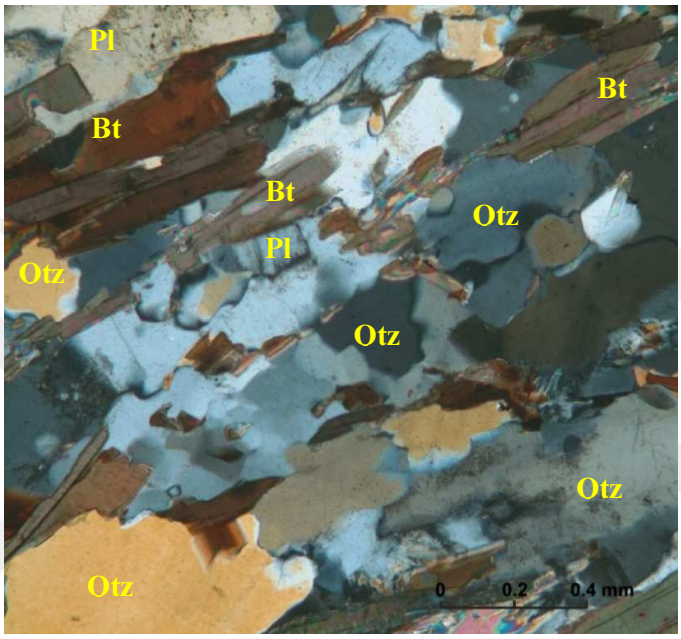

Figure 2.10: Micaschist, Sarıcakaya complex (~4.5 km north of Sarıcakaya town). Qtz: Quartz, Bt: Biotite, Pl: Plagioclase.

The a*mphibolite* is well foliated, fine to medium grained (0.2-2 mm). It consists mainly of plagioclase, amphibole, and minor quartz, biotite and opaque minerals (Figure 2.11). Plagioclase locally occurs as inclusions in hornblende. Opaque mineral is common and associated with hornblende.

The *metagranite* is well-foliated, and fine to medium grained (0.12-1 mm). It is mainly consisting of quartz, plagioclase, orthoclase, and minor muscovite and biotite. In addition, secondary sericite also developed (Figure 2.12).

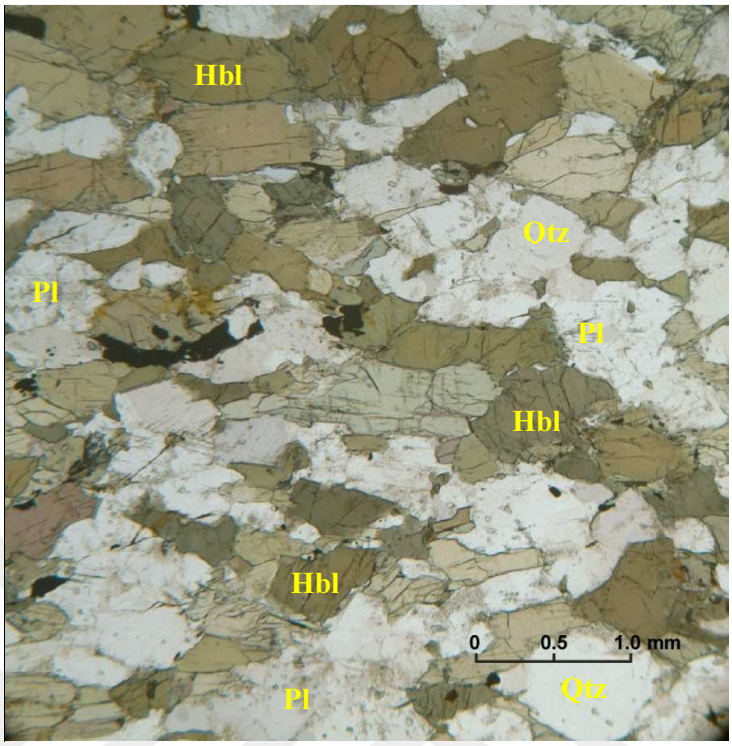

Figure 2.11: Amphibolite within Sarıcakaya metamorphic rocks (~5 km north of the Sarıcakaya town). Pl: Plagioclase, Hbl: Hornblende, Qtz: Quartz.

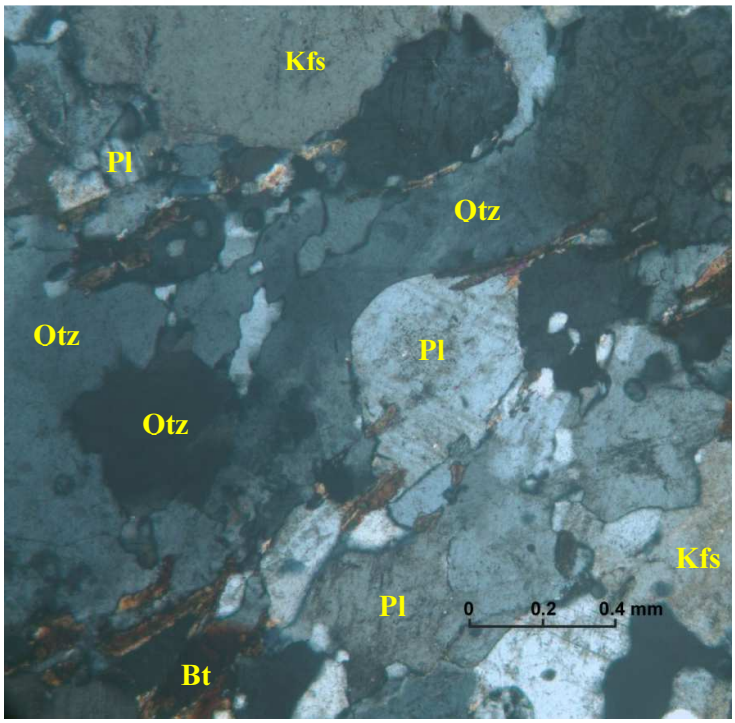

Figure 2.12: Foliated metagranite, Sarıcakaya complex (~3.7 km north of Çayköy village). Qtz: Quartz, Ms: Muscovite, Bt: Biotite, Pl: Plagioclase, Kfs: Potassium feldspar.

2.3. The Sarıcakaya Intrusive Rocks

2.3.1. Quartz diorite

The quartz diorite forms east-west trending sill-like exposure, ~20 km long and ~3 km across, (Figure 2.1), thus forming the biggest intrusive body in the study area. It is highly weathered and/or altered in places. A dark to greenish grey color is characteristic at the outcrops, grain size ranges from medium to coarse (0.5-5.1 mm). The quartz diorite is mainly massive. However, a feeble foliation can be recognized in some places. There are up to 10 cm thick mafic microgranular enclaves (Figure 2.13). They are usually round to angular in shape. The contact between mafic microgranular enclaves and host are mostly sharp. Quartz-diorite often cross cut by 0.5 – 50 cm thick aplitic and pegmatitic veins. The aplitic veins have a dirty-sugary appearance (Figures 2.14). The pegmatitic veins have pink colour due to abundance of orthoclase. The boundary between the veins and the host rock is mostly sharp, suggesting that the emplacement of the veins occur after the solidification of the host mafic rock.

Figure 2.13: A round mafic microgranular enclave (~10 cm) in quartz-diorite. Note the sharp boundary between the mafic microgranular enclave and host quartz diorite.

Figure 2.14: Two aplitic veins (~10 cm thick) cross-cut the massive quartz diorite. Note the sharp contact between the aplite and host quartz diorite (~5 km north-west of Sarıcakaya town).

The quartz diorite is composed of plagioclase, amphibole, biotite, quartz, and accessory phases such as opaque mineral (ilmenite), apatite, zircon (Figure 2.15). Secondary minerals are sericite (white mica), and chlorite. These secondary minerals formed from the alteration of biotite and plagioclase, respectively. Locally the amount of quartz increases, thus the quartz diorite grades into tonalite. Opaque minerals occur as inclusion in amphibole and biotite.

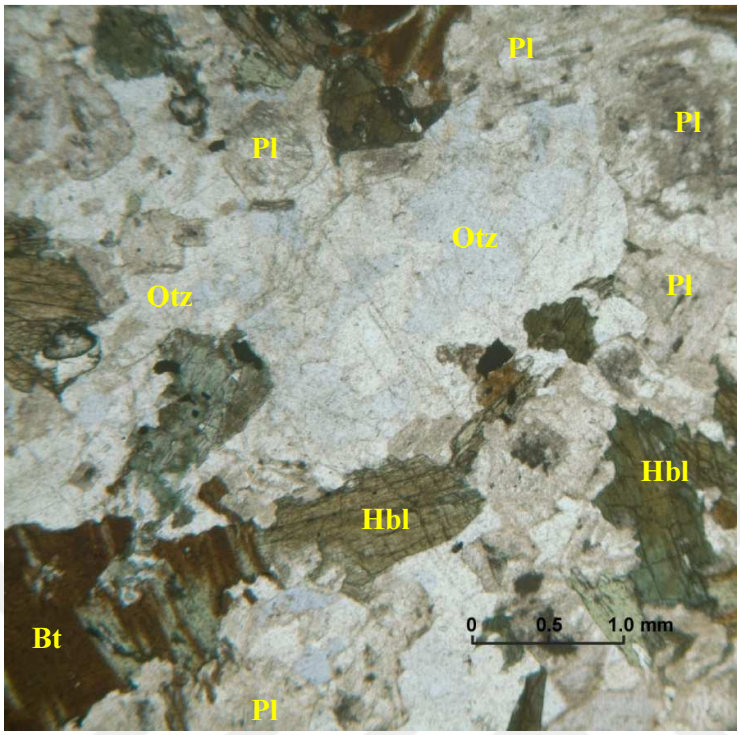

Figure 2.15: Quartz diorite. Sarıcakaya intrusive. Qtz: Quartz, Pl: Plagioclase Hbl: Hornblende, Bt: Biotite.

2.3.2. Hornblende-biotite-granite

The hornblende-biotite granite crops out in three isolated bodies, the largest one crop out in form of elongated body, 10 km long and 2 km across. Its actual form is concealed by overlying Middle Jurassic limestone (Figure 2.1). This unit is extremely altered/weathered so that a fresh sample cannot be taken. The rock type is characterized by pinkish to light gray color and medium grain sizes (1-3 mm). Massive texture is characteristic.

This rock displays equigranular texture, and consists of plagioclase, K-feldspar, quartz, biotite and amphibole (Figure 2.16). Opaque mineral, apatite and zircon are accessory minerals. Sericite and chlorite are secondary minerals. Feldspar generally displays subhedral to euhedral, tabular crystals. Generally they slightly transformed to sericite, and some crystals show zoning features. Quartz is abundant and generally has anhedral shape. Biotite crystals transformed to chlorite along their cleavage. Hornblende generally display tabular shapes and contain inclusions of feldspar and opaque mineral.

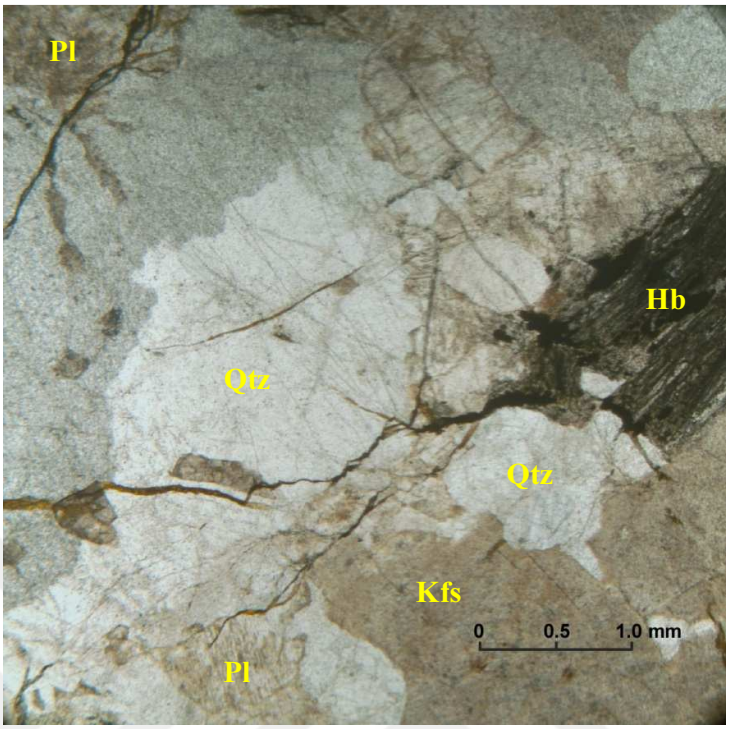

Figure 2.16: Hornblende-biotite granite, Sarıcakaya intrusive (~2.6km south west of Akkoy village). Qtz: Quartz, Pl: Plagioclase, Hbl: Hornblende, Kfs: Potassium feldspar.

2.3.3. Leucogranite

The leucogranite crops out throughout the study area in form of dikes/sills (1 to 50 m. thick) to small stocks (~800m across) in the metamorphic rocks (Figure 2.1; 2.17). The rocks are leucocratic. The outcrop color changes from white dirty to light yellow and light brown. Leucogranites are massive, and devoid of any pervasive texture. Graphic intergrowths can be recognized in the field. Grain sizes are not uniform, changing from aplitic to pegmatitic ones (1mm to 2 cm). Garnet and muscovite occur locally.

The leucogranite consists mainly of orthoclase, plagioclase, quartz, and minor garnet and muscovite (Figure 2.18). Quartz grains, are generally anhedral, and show undulatory extinction and sutured outlines, besides locally they are slightly elongate. Plagioclase has anhedral grain boundaries. Garnet forms round grains (anhedral), fine to medium grains (200 µm to 3 mm). Muscovite is common and forms fine grained flakes. There are rare alteration products of sericite and chlorite.

Figure 2.17: A sill of garnet-muscovite bearing leucocratic granite (~1.5 m thick) within the metamorphic rocks (~5.7 km north of Sarıcakaya town).

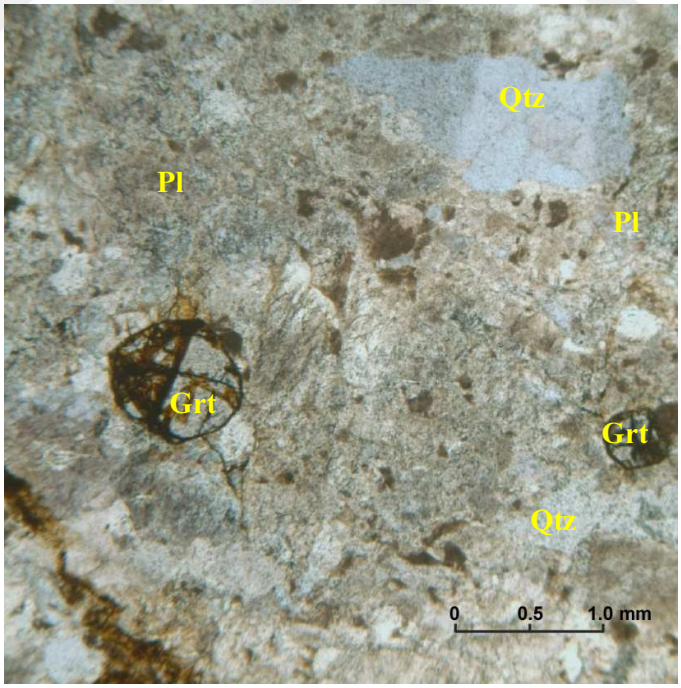

Figure 2.18: Rounded garnet grain in the leucogranite (~1km north east of Tozman village). Qtz: Quartz, Pl: Plagioclase, Ms: Muscovite, Grt: Garnet.

2.3.4. Muscovite-biotite granite

The two mica granite forms a small stock in the metamorphic rocks in the northern part of the study area (~ 0.8 km long and 0.5 km across) (Figure 2.1). It displays a dark grey color, and fine to medium grain sizes (0.2-2 mm). The rock is mainly massif, but a weak foliation can be recognized. In contrast to garnet-muscovite granite, grain size distribution is relatively homogenous.

It consists mainly of quartz, plagioclase, muscovite, biotite and K-feldspar (orthoclase and microcline) (Figure 2.19). Plagioclase irregular grain boundaries and locally transformed to sericite. Besides; quartz also show anhedral shapes, slightly elongated and has sutured edges. The shape of microcline are generally subhedral to anhedral. Garnet is not common in these rocks and when it can be detected it forms fine, rounded grains.

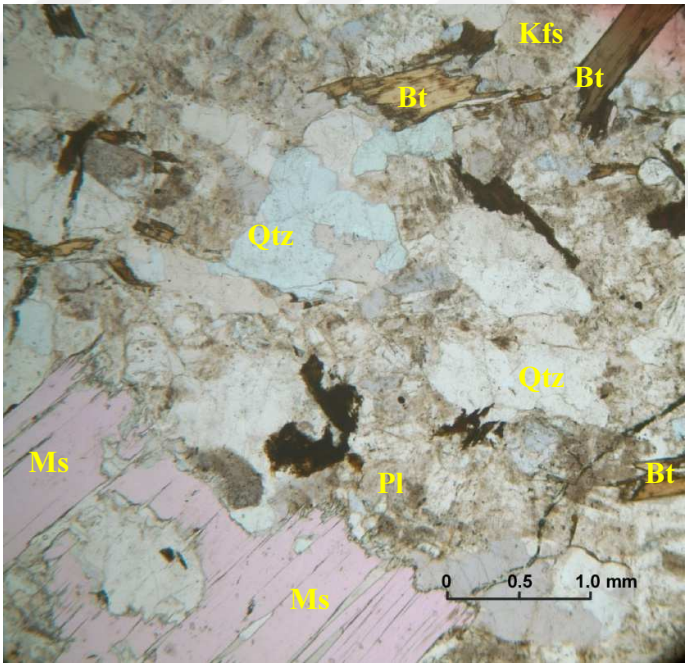

Figure 2.19: Muscovite-biotite granite (~1.6 south of Akköy village). Ms: Muscovite, Bt: Biotite, Kfs: K-feldspar, Pl: Plagioclase, Qtz: Quartz.

2.3.5. Cumulate gabbro-peridotite complexes

It crops out in form of small stocks (the largest one up to 3 km across) at several locations within the metamorphic rocks (Figure 2.1). It is dark grey to black in colour, fine to medium grained (1-2 mm) (Figure 2.20). It is slightly transformed to serpentinite. Around the intrusions a pronounced contact metamorphic aureole is developed. The complex is made up gabbro to peridotite.

Figure 2.20: Field appearance of the cumulate rocks (~3 km north of Çayköy village, Sarıcakaya complex).

Cumulate peridotite (Lherzolite) is fine to medium grained (0.5-1.2 mm), and consists mainly of olivine and clinopyroxene, amphibole, in addition to orthopyroxene. Cumulate texture is characteristic. Relatively large crystals of pyroxene and amphibole (intercumulus phases) enclose numerous smaller crystals of olivine (cumulus phase) (Figure 2.21). These olivine crystals form rounded to well-rounded grains, generally fractured. Secondary chlorite, opaque, serpentine developed in cracks (Sieve texture).

The cumulate gabbro is fine to medium grained (0.2-1.8 mm), massif and displays cumulate texture. It consists of plagioclase, clinopyroxene and hornblende, in addition to biotite and opaque mineral. Secondary minerals are sericite and chlorite. Plagioclase and clinopyroxene are cumulus minerals. Intercumulus hornblende fills the interstitial spaces (Figure 2.22).

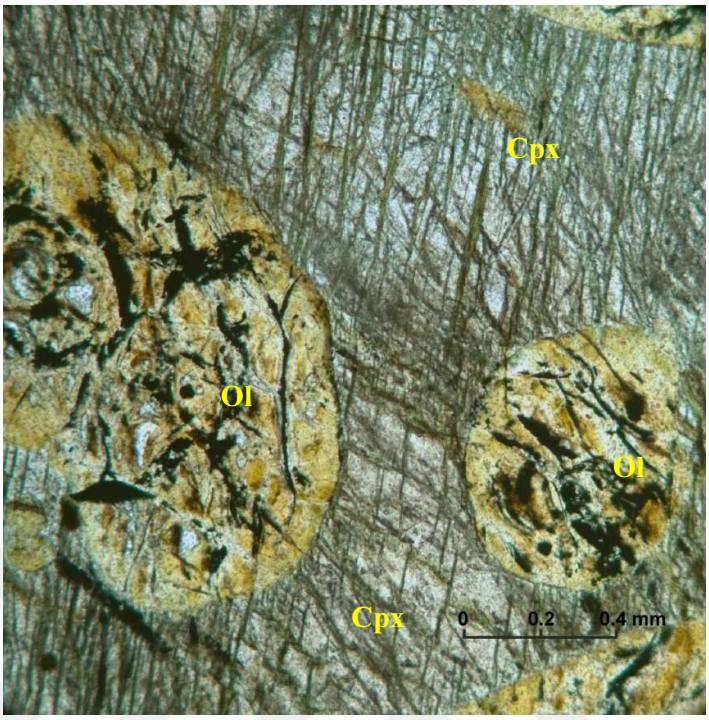

Figure 2.21: Cumulus olivine surrounded by intercumulus clinopyroxene in cumulate peridotite. (~2.3 north of Çayköy village). Ol: Olivine, Cpx: Clino-pyroxene.

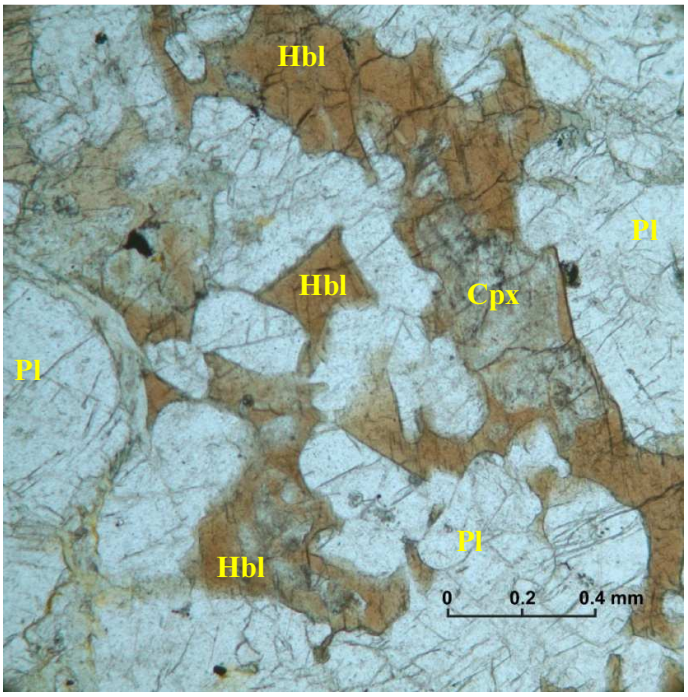

Figure 2.22: Intercumulus hornblende (Hbl) surrounds cumulus plagioclase (Pl) and clino-pyroxene (Cpx). The crystallization sequence is plagioclase, clinopyroxene and hornblende (~2.3 north of Çayköy village).

3. GEOCHEMISTRY

In order to characterize the geochemical features of the Sarıcakaya intrusive rocks, 35 samples have analyzed. The bulk geochemical data is given in Tables 3.1 and 3.2. Geochemical characteristics of each rock type is discussed below separately.

3.1. Quartz Diorite

The quartz diorite displays a narrow compositional variation (SiO_2 = 59-63 wt%, Al_2O_3 = 17 – 18 wt%, FeO* = 5.20 – 6.28 wt%, MgO = 2.63 – 3.52 wt%, Na_2O = 2.5 – 3 wt%, K_2O = 1.8 – 2.8 wt% (Table 3.1). The quartz diorite plots in the diorite field on total $K_2O + Na_2O$ vs. SiO_2 diagram of Cox et al (1979) (Figure 3.1), which is in line with the petrographic examinations. In the SiO_2 vs. K_2O diagram of Peccerillo and Taylor (1976), the samples straddle on the divide between the medium to high-K calc-alkaline fields (Figure 3.2). The quartz diorite shows high CaO (4.78 – 6.72 wt%) relative to Na_2O and K_2O (Table 3.1). The aluminum saturation index [ASI = molar $Al_2O_3/(CaO + Na_2O + K_2O)$] ranges from 0.95 to 1.05 (Figure 3.3). Higher values of ASI is probably related to formation of secondary minerals such as sericite and chlorite. Magnesium number [Mg# =100* molar MgO/ (molar MgO + molar FeO_{tot})] ranges from 46.5 to 50. Hornblende bearing nature of the quartz diorite is consistent with its metaluminous nature. Despite the narrow compositional variation, abundance of Al_2O_3, Fe_2O_{3tot}, MgO, CaO, Sr and Y decrease with increasing SiO_2 (Figure 3.2; 3.5).

Table 3.1: Whole-rock analyses of selected samples of quartz diorite from the Sarıcakaya intrusive.

Samples	57a	67	70	123	125	126a	134a	196a	202	207a	69
Rock type	QD	QD	QD	QD	QD	QD	QD	QD	QD	QD	QD
SiO_2	62.69	62.23	61.11	58.94	58.55	59.43	60.25	61.44	59.99	60.08	61.16
TiO_2	0.63	0.64	0.71	0.74	0.71	0.65	0.61	0.82	0.69	0.69	0.60
$Al2O_3$	16.46	16.46	16.50	17.02	17.68	17.89	17.66	16.74	16.94	17.05	16.86
$Fe2O_3$	5.77	6.17	6.53	6.97	6.86	6.02	5.97	5.77	6.49	6.39	5.92
FeO	5.20	5.56	5.88	6.28	6.18	5.42	5.38	5.20	5.85	5.76	5.33
MnO	0.10	0.10	0.11	0.12	0.12	0.10	0.10	0.11	0.11	0.10	0.11
MgO	2.63	2.82	2.97	3.52	3.25	2.74	2.78	2.68	3.15	2.81	2.63
CaO	4.78	5.20	5.74	5.62	6.64	6.25	6.72	4.94	5.86	5.77	4.85
Na_2O	2.65	2.84	2.54	2.47	2.62	2.62	2.63	2.99	2.71	2.65	2.90
K_2O	2.88	2.11	2.09	2.27	1.82	2.22	1.80	2.36	1.94	2.28	2.29
P_2O_5	0.10	0.11	0.11	0.12	0.12	0.10	0.11	0.15	0.10	0.10	0.11
LOI	1.10	1.10	1.40	2.00	1.40	1.70	1.20	1.70	1.80	1.90	2.30
Cr_2O_3	0.00	0.01	0.01	0.01	0.01	0.01	0.01	0.01	0.01	0.01	0.01
Total	99.80	99.81	99.82	99.79	99.79	99.79	99.80	99.75	99.81	99.80	99.77
Sc	19	20	22	22	24	20	22	14	22	20	18
Ni	5.7	13.7	12.7	10.9	8.5	32.7	13.3	20.3	8.9	7.7	31.1
Co	12.3	14	14.4	15.6	16.3	14.8	14.2	14.1	15	14	13.3
V	108	109	126	136	143	123	128	92	134	131	96
Cu	13.3	8.5	10.5	12.4	10.2	13.7	12.7	3.5	13.3	6.9	24.9
P	218.19	240.01	240.01	261.83	261.83	218.19	240.01	327.29	218.19	218.19	240.01
Zn	46	50	49	51	48	43	41	72	50	51	53
Cs	2.20	1.70	2.20	2.30	2.30	2.40	2.00	3.00	2.30	1.80	1.70
Rb	97.30	74.80	78.10	86.60	69.00	76.10	61.40	87.10	75.40	84.90	80.70
Ba	649.00	532.00	451.00	536.00	476.00	686.00	565.00	770.00	412.00	621.00	702.00
U	1.00	1.30	1.30	0.80	0.70	0.90	1.50	1.30	1.70	1.10	0.60
Th	10.10	6.70	1.70	3.00	28.10	0.40	13.30	14.10	2.70	4.80	22.60
Pb	4.80	3.00	3.30	4.20	2.90	4.20	3.50	4.90	4.10	3.30	4.70
Sr	261.30	265.00	251.30	276.80	308.80	322.80	300.00	415.10	287.40	262.80	291.30
Nb	9.90	9.50	8.90	8.00	8.60	6.90	7.10	9.40	8.10	8.00	9.20
Ta	0.60	0.50	0.50	0.70	0.60	0.50	0.50	0.50	0.70	0.60	0.50
Zr	152.50	140.50	117.50	146.90	161.00	136.80	110.80	177.30	131.40	146.40	120.70
Hf	4.70	3.80	3.60	4.00	4.50	3.70	3.20	4.60	4.10	4.00	3.20
Y	18.90	22.10	22.30	20.90	26.40	20.10	24.00	12.70	23.70	20.70	19.70
La	27.00	25.40	9.60	12.90	14.80	8.30	38.10	55.80	13.20	15.80	77.00
Ce	50.70	47.80	21.90	31.60	34.40	19.40	71.60	103.50	29.40	32.30	134.40
Pr	5.75	5.53	3.32	4.2	4.96	3.06	7.56	10.59	3.87	4.22	12.76

Rock type: QD=quartz diorite, Mg# = 100*(MgO / MgO+FeO_{tot}) in molar proportions, ASI = Aluminum saturation index = Molar Al_2O_3 / (CaO+Na_2O+K_2O), (La/Yb)cn = chondrite-normalized La/Yb ratio, oxides are given in wt%, trace elements in ppm.

Table 3.1 (continued): Whole-rock analyses of selected samples of quartz diorite from the Sarıcakaya intrusive.

Samples	57a	67	70	123	125	126a	134a	196a	202	207a	69
Rock type	QD	QD	QD	QD	QD	QD	QD	QD	QD	QD	QD
Nd	21.8	20.9	15.6	17.2	20.9	14.1	27.2	35.8	15.8	17.4	38.6
Sm	4.33	4.5	4.07	3.87	5.02	3.51	4.82	4.96	4.11	3.9	5.61
Eu	0.94	1.12	1.02	1	1.17	1.03	1.18	1.31	1.02	1.07	1.14
Gd	3.94	4.52	4.01	4.07	5.16	3.8	4.68	3.92	4.09	3.96	4.5
Tb	0.63	0.75	0.68	0.67	0.82	0.62	0.72	0.52	0.68	0.68	0.68
Dy	3.63	4.4	4.1	3.84	5	3.84	4.03	2.63	3.84	3.74	3.81
Ho	0.8	0.84	0.83	0.8	0.96	0.71	0.83	0.49	0.83	0.78	0.76
Er	2.1	2.57	2.45	2.17	2.87	2.21	2.38	1.24	2.41	2.19	2.02
Tm	0.29	0.36	0.34	0.33	0.41	0.33	0.37	0.17	0.34	0.34	0.3
Yb	1.94	2.44	2.25	2.1	2.62	1.98	2.3	1.09	2.38	2.06	1.84
Lu	0.33	0.36	0.35	0.33	0.39	0.31	0.35	0.18	0.36	0.33	0.28
Mg#	47.42	47.49	47.37	49.98	48.38	47.38	47.95	47.89	48.99	46.53	46.78
ASI	1.02	1.00	0.98	1.02	0.96	0.99	0.95	1.02	0.98	0.98	1.05
(La/Yb)cn	9.38	7.02	2.88	4.14	3.81	2.83	11.17	34.51	3.74	5.17	28.21
Eu/Eu*	0.68	0.75	0.76	0.77	0.70	0.86	0.75	0.88	0.75	0.83	0.67

Rock type: QD=quartz diorite, Mg# = 100*(MgO / MgO+FeO_{tot}) in molar proportions, ASI = Aluminum saturation index = Molar Al_2O_3 / (CaO+Na_2O+K_2O), (La/Yb)cn = chondrite-normalized La/Yb ratio, oxides are given in wt%, trace elements in ppm.

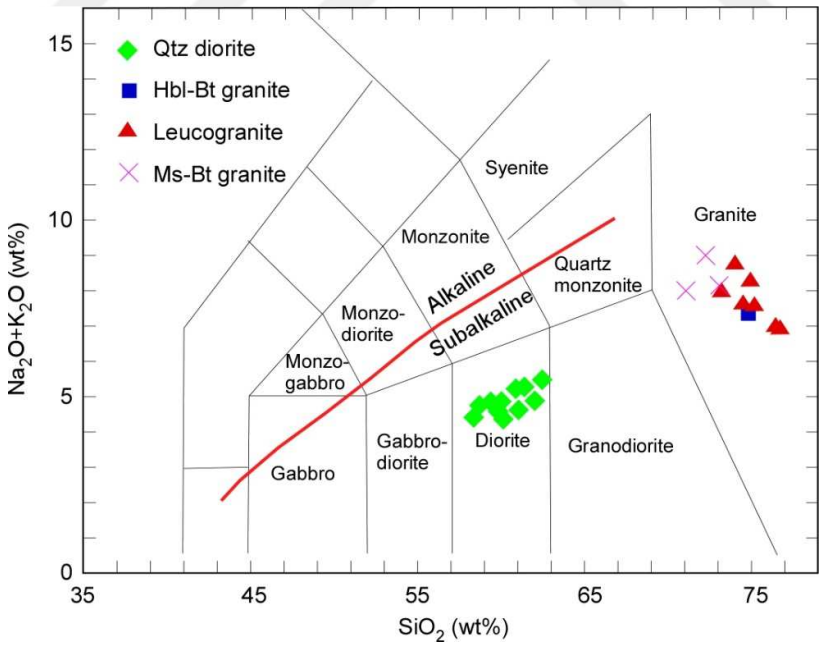

Figure 3.1: Locations of the different type of the intrusive rocks from the Sarıcakaya on SiO_2 vs Na_2O + K_2O (TAS Diagram) (after Cox et al, 1979).

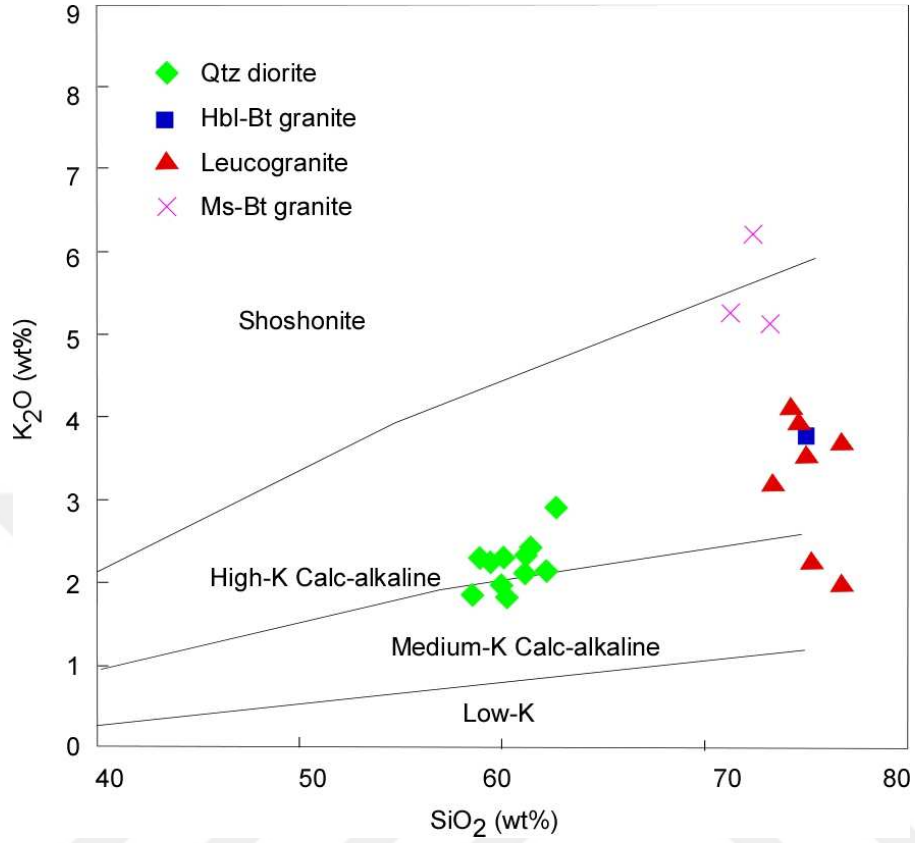

Figure 3.2: Locations of the different type of the intrusive rocks from the Sarıcakaya on SiO_2 vs K_2O (after Peccerillo & Taylor 1976).

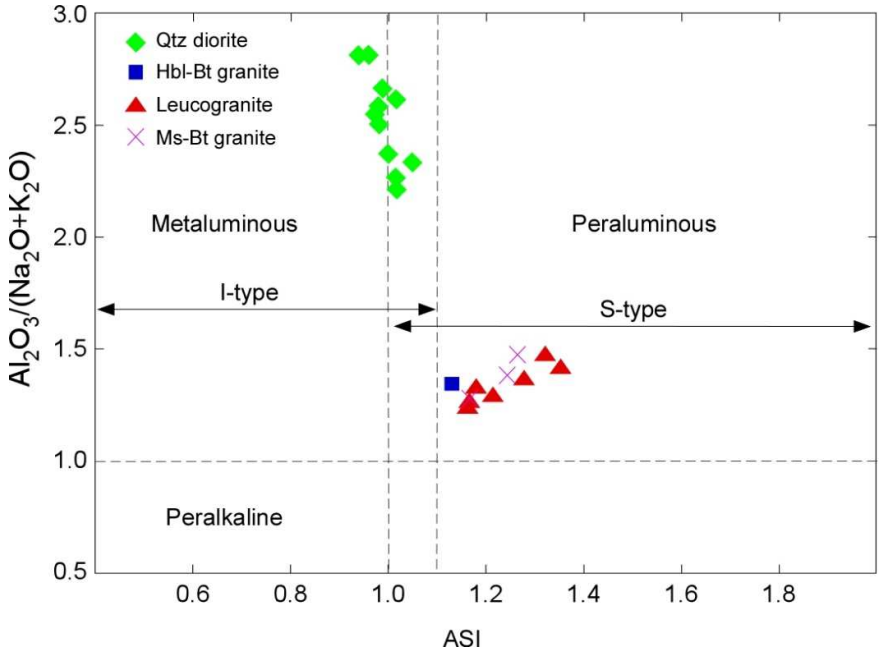

Figure 3.3: Locations of the different type of the intrusive rocks from the Sarıcakaya on ASI vs $Al_2O_3/(Na_2O+K_2O)$ diagram (after De la Roche et al, 1980).

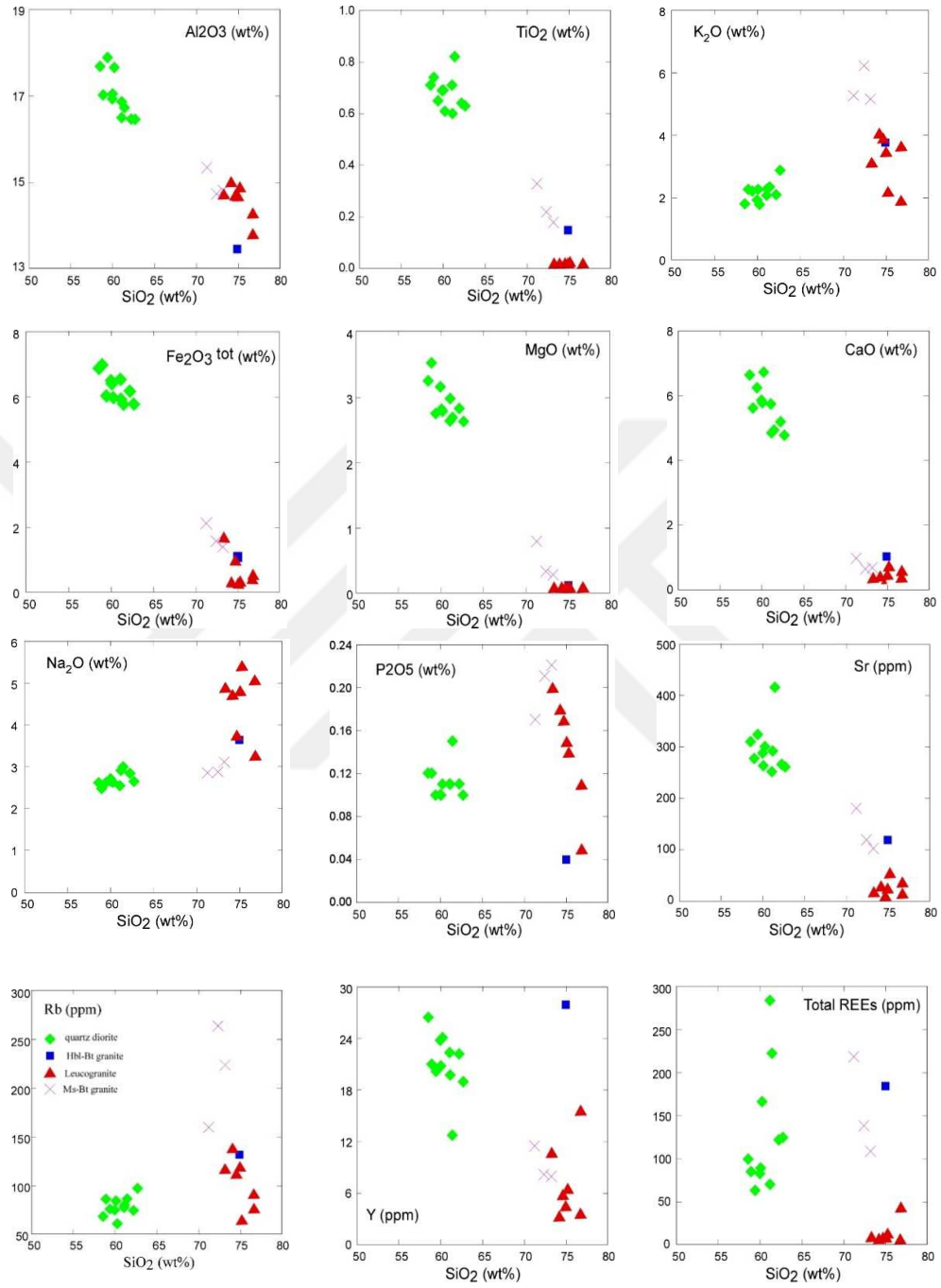

Figure 3.4: Selected Harker variation diagrams for the different intrusive from the Sarıcakaya complex.

Chondrite-normalized (cn) rare earth element (REE) patterns of the quartz diorite samples are generally characterized by relatively fractionated rare earth element patters, and concave-upward shape of middle to heavy rare earth elements. Depending on the forms of the rare earth elements, quartz diorites are divided into three types.

(i) Type-I: The samples 57a, 67, 69 and 134a (Figure 3.5) show enrichment in light rare earth elements, LREEs [$(La/Yb)_{cn}$ = (La_{sample} /$La_{Chondrite}$)/(Yb_{Sample}/$Yb_{Chondrite}$)] ranging from 7.02 – 28.21 and they have nearly flat heavy rare earth elements, HREEs pattern [$(Gd/Yb)_{cn}$ = (Gd $_{sample}$ /Gd $_{Chondrite}$) / Yb $_{sample}$ / Yb $_{Chondrite}$)] range from 1.53 – 2.02 with pronounced negative Eu anomaly [Eu/Eu* = Eu_{cn} / 0.5*(Sm_{cn}+Gd_{cn})] = 0.67 – 0.75] (Figure 3.5). These features can be accounted for by a fractionating mineral assemblage of garnet, plagioclase, hornblende and pyroxene.

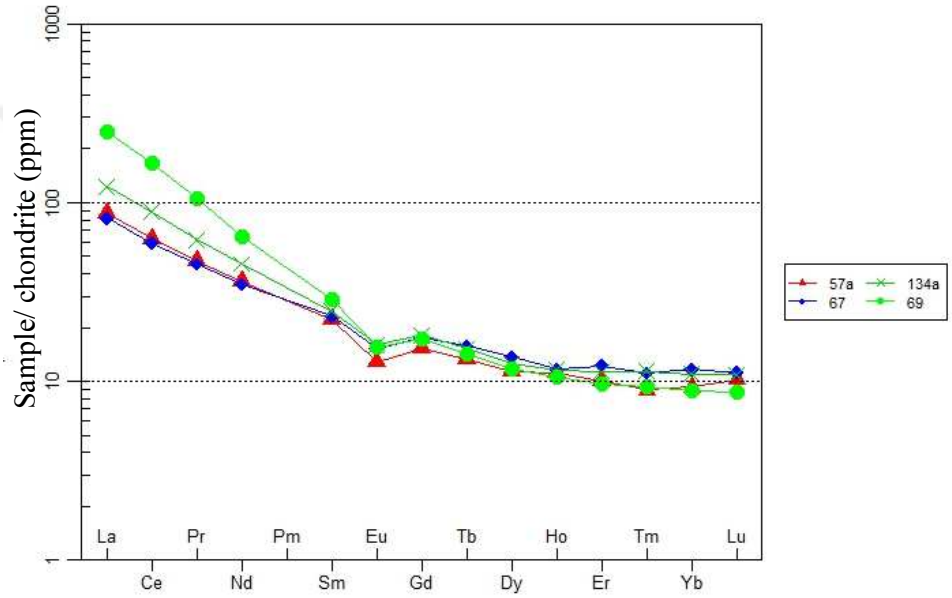

Figure 3.5: Type-I quartz diorite samples. Chondrite-normalized rare earth element diagram. Normalizing values were taken from Boynton (1984).

(ii) Type-II: Samples 70, 123, 125, 126a, 202 and 207a show less enrichment in LREEs [$(La/Yb)_{cn}$ = 2.83 – 5.17] and they have nearly flat HREEs pattern as well [$(Gd/Yb)_{cn}$ = 1.42-1.63] with generally less pronounced negative Eu anomaly [Eu/Eu* = 0.70 – 0.86] (Figure 3.6). Slightly fractionated nature of the rare earth elements rules out the presence of garnet in the source.

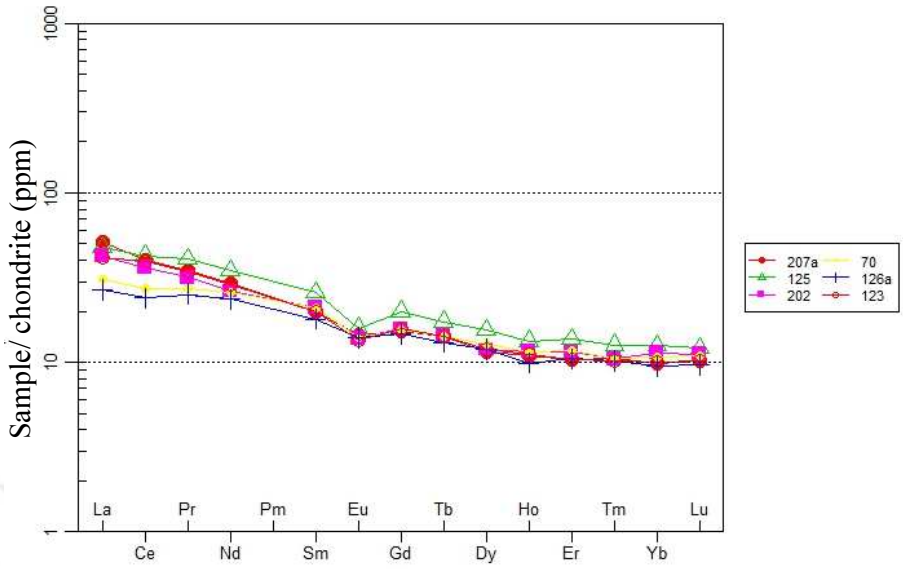

Figure 3.6: The type-II quartz diorite samples. Chondrite-normalized rare earth elements diagram. Normalizing values were taken from Boynton (1984).

(iii) Type-III: Sample 196a is an exception, it shows high enrichment in LREEs and high depletion in HREEs with chondrite normalized La/Yb ratios of 34.51 and a feeble negative Eu anomaly (Eu/Eu*= 0.88) (Table 3.1, Figure 3.7). This can be indicates fractionation of garnet and hornblende from the melt.

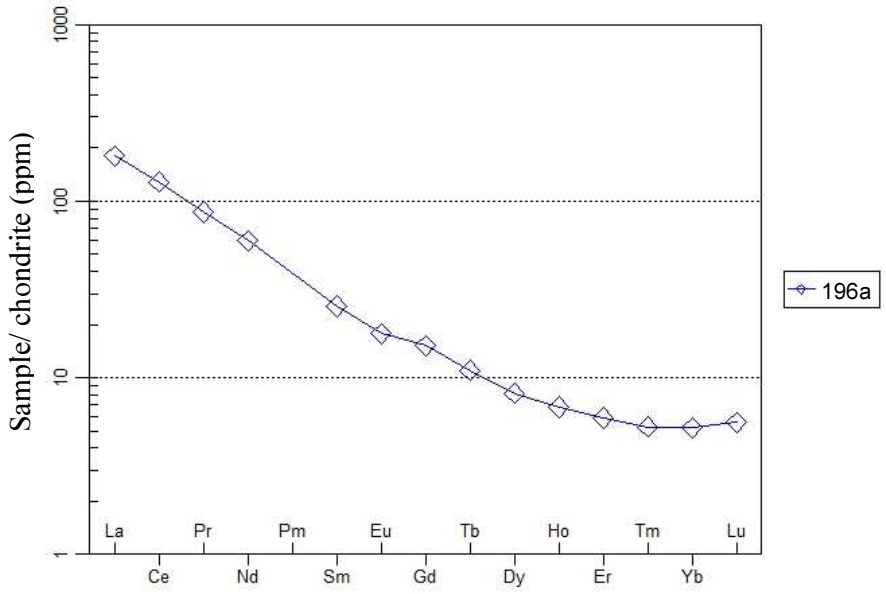

Figure 3.7: Type-III quartz diorite sample. Chondrite-normalized rare earth element diagram. Normalizing values were taken from Boynton (1984).

On multi-element variation diagrams normalized to primitive mantle ($MEVD_{pmn}$) after Sun and McDonough, (1989). (i) Type-I samples 57a, 67, 69 and 134a display marked negative anomalies in Nb, P and Ti but positive anomalies in Th, K, Pb and Nd (Figure 3.8). Negative anomalies in Nb, P and Ti can be explained by fractionation of apatite, sphene and rutile. (ii) Type-II samples 70, 123, 125, 126a, 202, and 207a show negative anomalies in Th (except sample 125 which shows positive Th anomaly), Nb, P and Ti but positive anomalies in K, Pb, and Zr (Figure 3.9). (iii) The sample 196a shows marked negative anomalies in Nb and P, but positive anomalies in Th and Nd (Figure 3.10).

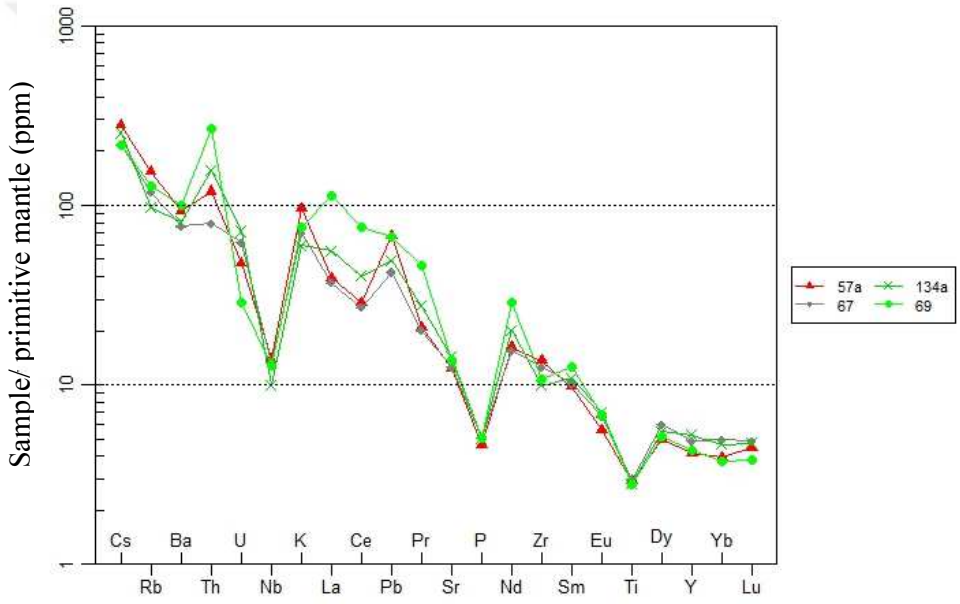

Figure 3.8: Type-I quartz diorite samples, Primitive mantle-normalized element abundance patterns. For normalizing values and sequence of elements, see (Sun and McDonough, 1989).

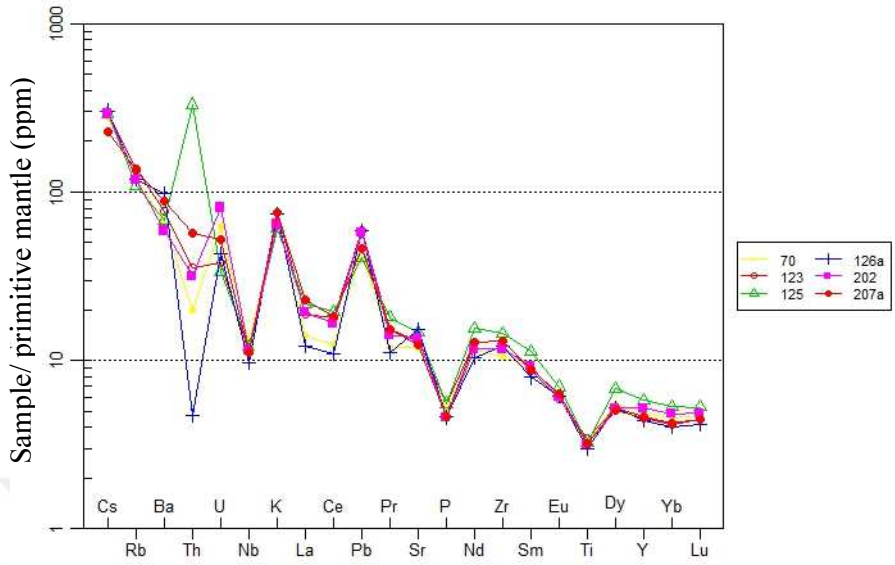

Figure 3.9: Type-II quartz diorite samples. Primitive mantle-normalized element abundance patterns. For normalizing values and sequence of elements, see Sun and McDonough (1989).

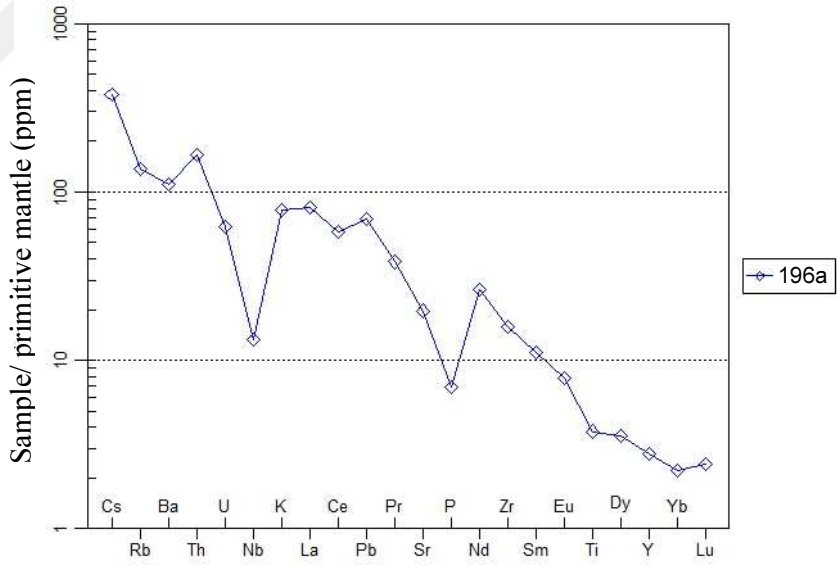

Figure 3.10: Type-III quartz diorite sample. Primitive mantle-normalized element abundance patterns. For normalizing values and sequence of elements, see Sun and McDonough (1989).

3.2. Biotite-hornblende Granite

The biotite-hornblende granite is extensively weathered and/or altered. Hence only one sample is suitable for geochemical analysis. This sample is characterized by the composition such as SiO_2 = 74.96 wt%, Al_2O_3 = 13.46 wt%, FeO* = 0.98 wt%, MgO = 0.1wt%, Na_2O = 3.63 wt%, K_2O = 3.76 wt% (Table 3.2). The biotite-hornblende granite plots in the granite field on total $K_2O + Na_2O$ vs. SiO_2 (TAS) diagram (Figure 3.11). This is also in line with the petrography. The aluminum saturation index (ASI) and Mg number are 1.13 and 15.36, respectively. So this rock is peraluminous. In the SiO_2 vs. K_2O diagram after Peccerillo & Taylor (1976) the sample falls in the high-K calc-alkaline field (Figure 3.2).

$REE_{(cn)}$ patterns of the biotite-hornblende granite (only one sample is analyzed) is characterized by concave-upward shape (Figure 3.11). It shows slight enrichment in LREEs relative to HREEs [$(La/Yb)_{cn}$ = 9.92], ruling out significant involvement of garnet in the formation. This rock has nearly flat HREE pattern (Gd/Yb_{cn} = 1.47). REEs pattern shows pronounced negative Eu anomaly (Eu/Eu* = 0.42) indicating fractionation of plagioclase (Table 3.2; Figure 3.11).

Table 3.2: Whole-rock analyses of selected samples of different granites from the Sarıcakaya intrusive.

Samples	113	37b	110b	140	141	142	211	219	25	161a	185
Rock type	BHG	LG	LG	LG	LG	LG	LG	LG	MBG	MBG	MBG
SiO_2	74.96	76.80	74.67	73.34	74.22	76.75	75.27	75.02	72.43	71.28	73.24
TiO_2	0.15	0.01	0.01	0.01	0.01	0.01	0.02	0.01	0.22	0.33	0.18
$Al2O_3$	13.46	13.82	14.72	14.75	15.02	14.30	14.90	14.69	14.74	15.34	14.82
Fe_2O_3	1.09	0.56	1.00	1.71	0.33	0.44	0.36	0.30	1.57	2.11	1.40
FeO	0.98	0.50	0.90	1.54	0.30	0.40	0.32	0.27	1.41	1.90	1.26
MnO	0.02	0.13	0.41	0.54	0.06	0.09	0.02	0.02	0.02	0.03	0.02
MgO	0.10	0.06	0.07	0.08	0.04	0.07	0.06	0.05	0.32	0.78	0.27
CaO	1.03	0.60	0.26	0.38	0.43	0.40	0.74	0.49	0.63	0.97	0.68
Na_2O	3.63	3.27	3.75	4.89	4.72	5.08	5.41	4.82	2.88	2.84	3.10
K_2O	3.76	3.67	3.91	3.15	4.08	1.94	2.22	3.49	6.22	5.27	5.15
P_2O_5	0.04	0.05	0.17	0.20	0.18	0.11	0.14	0.15	0.21	0.17	0.22
LOI	1.70	1.00	1.00	1.00	0.90	0.80	0.90	1.00	0.70	0.70	0.80
Cr_2O_3	<0.002	0.00	0.01	0.00	<0.002	0.00	<0.002	<0.002	0.01	0.00	0.01
Total	99.88	99.99	99.99	100.00	100.00	99.99	99.99	100.00	99.90	99.84	99.93
Sc	5	2	<1	<1	<1	<1	<1	<1	3	4	2
Ni	1.7	10.8	18.2	10.1	6.7	8.5	2.4	6	16.2	8.5	15.1
Co	1	0.6	0.5	0.3	0.2	0.5	0.3	0.2	2	3.1	1.6
V	<8	<8	<8	<8	<8	<8	12	<8	14	34	13
Cu	4.1	3.7	12.4	3.4	3.5	4	4	2	4.6	12.8	3.3
P	87.28	109.10	370.92	436.38	392.74	240.01	305.47	327.29	458.20	370.92	480.02
Zn	34	3	5	4	3	2	8	5	56	50	48
Cs	2.50	0.40	1.00	0.60	0.80	1.20	0.50	0.80	5.00	6.60	6.90
Rb	131.90	77.60	112.70	117.70	138.60	92.20	65.20	119.70	263.60	159.30	223.60
Ba	681.00	92.00	13.00	50.00	43.00	12.00	44.00	19.00	416.00	692.00	300.00
U	3.10	1.50	5.00	1.30	1.10	3.60	3.10	2.00	4.90	7.30	8.30
Th	13.40	2.40	0.40	0.20	0.20	0.20	0.50	0.20	14.70	22.30	10.20
Pb	6.10	5.70	5.40	5.70	7.10	1.80	12.20	8.90	3.80	2.50	2.70
Sr	119.00	37.20	5.80	16.90	30.60	15.30	55.60	25.50	118.60	180.70	102.20
Nb	8.70	7.60	0.50	1.90	1.10	3.30	4.50	3.40	13.40	11.00	11.70
Ta	0.90	1.20	0.30	0.30	0.20	0.40	0.70	0.30	1.30	0.90	1.00
Zr	134.70	25.40	106.10	29.80	32.70	56.30	15.00	27.50	80.10	110.70	61.60
Hf	4.10	1.50	5.10	1.60	1.40	2.60	0.80	1.10	2.70	3.40	2.20
Y	27.90	15.60	5.80	10.70	3.30	3.60	6.50	4.50	8.10	11.40	7.90
La	42.10	7.50	2.40	1.20	1.50	1.60	3.50	1.70	27.10	45.50	22.50
Ce	78.10	16.20	2.10	2.40	2.40	2.30	4.10	3.10	61.30	99.40	46.90
Pr	8.67	1.87	0.24	0.26	0.25	0.28	0.48	0.35	7.13	11.53	5.55

Rock type: BHG = Biotite-hornblende granite, LG = Leucogranite, MBG = Muscovite-biotite granite, Mg# = 100*(MgO / ($MgO+FeO_{tot}$)) in molar proportions, ASI = Aluminum saturation index = Molar Al_2O_3 / ($CaO+Na_2O+K_2O$), (La/Yb)cn = chondrite-normalized La/Yb ratio, oxides are given in wt%, trace elements in ppm.

Table 3.2 (continued): Whole-rock analyses of selected samples of different granites from the Sarıcakaya intrusive.

Samples	113	37b	110b	140	141	142	211	219	25	161a	185
Rock type	BHG	LG	LG	LG	LG	LG	LG	LG	MBG	MBG	MBG
Nd	30.1	6.6	0.6	0.8	0.9	0.9	1.6	1.1	27.4	40.9	20.2
Sm	5.89	2.13	0.23	0.26	0.23	0.22	0.49	0.26	6.17	8.21	4.95
Eu	0.77	0.11	0.02	0.04	0.08	0.02	0.15	0.06	0.8	1.19	0.61
Gd	5.08	2.58	0.25	0.4	0.24	0.22	0.47	0.31	4.6	5.92	3.89
Tb	0.82	0.48	0.12	0.17	0.05	0.07	0.12	0.09	0.53	0.71	0.51
Dy	5.09	2.77	0.87	1.55	0.49	0.46	0.83	0.63	1.94	2.72	2.14
Ho	0.92	0.5	0.18	0.29	0.1	0.09	0.17	0.12	0.23	0.33	0.25
Er	2.9	1.5	0.49	0.88	0.36	0.34	0.66	0.42	0.53	0.8	0.55
Tm	0.42	0.21	0.09	0.16	0.07	0.08	0.11	0.08	0.07	0.11	0.06
Yb	2.86	1.37	0.83	1.21	0.6	0.76	0.83	0.65	0.4	0.76	0.42
Lu	0.45	0.2	0.12	0.17	0.1	0.11	0.16	0.08	0.06	0.1	0.05
Mg#	15.36	16.04	11.09	7.70	17.77	22.09	22.90	22.90	26.65	39.72	25.58
ASI	1.13	1.32	1.35	1.21	1.16	1.28	1.18	1.17	1.17	1.26	1.24
(La/Yb)cn	9.92	3.69	1.95	0.67	1.69	1.42	2.84	1.76	45.68	40.36	36.12
Eu/Eu*	0.42	0.14	0.25	0.38	1.03	0.28	0.94	0.65	0.44	0.50	0.41

Rock type: BHG = Biotite-hornblende granite, LG = Leucogranite, MBG = Muscovite-biotite granite, Mg# = 100*(MgO / ($MgO+FeO_{tot}$)) in molar proportions, ASI= Aluminum saturation index = Molar Al_2O_3 / ($CaO+Na_2O+K_2O$), (La/Yb)cn = chondrite-normalized La / Yb ratio, oxides are given in wt%, trace elements in ppm.

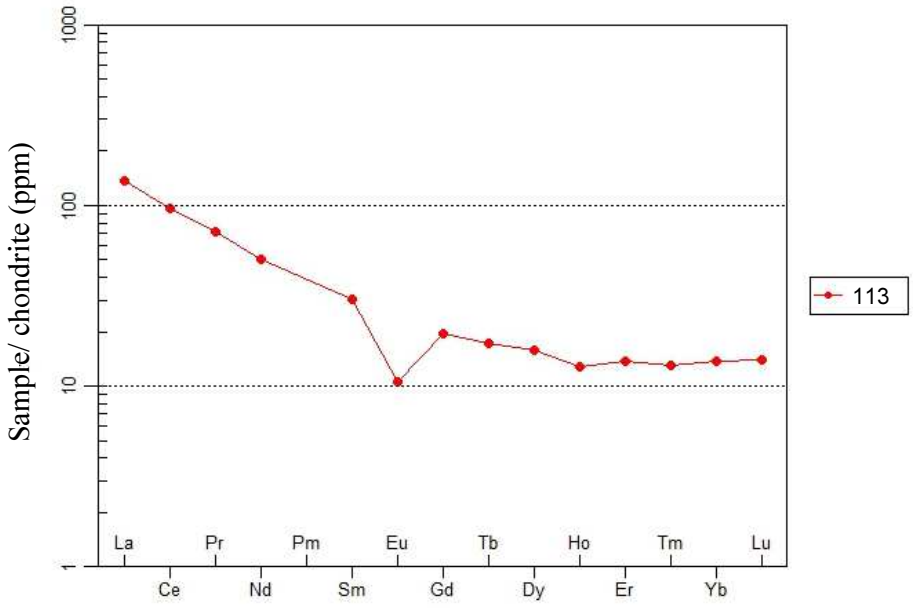

Figure 3.11: Biotite-hornblende granite sample. Chondrite-normalized rare earth element diagram. Normalizing values were taken from Boynton (1984).

On $MEVD_{(pmn)}$, the biotite-hornblende granite displays pronounced negative anomalies in Ba, Nb, Sr, P, Eu and Ti. Depletion in P and Ti could be controlled by

individual minerals such as apatite, ilmenite, sphene and rutile. It has positive anomalies in K, Pb, Nd and Sm (Figure 3.12).

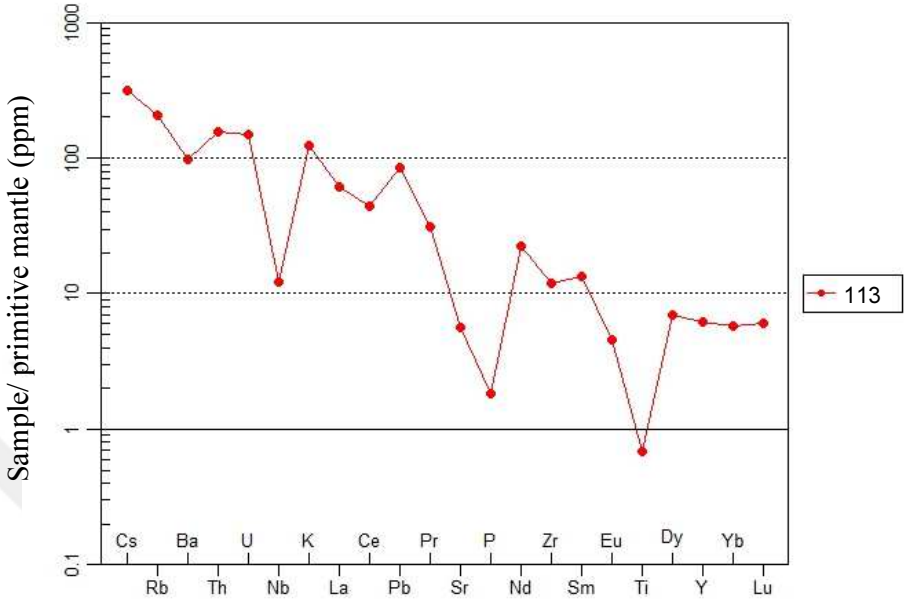

Figure 3.12: Biotite-hornblende granite sample. Primitive mantle-normalized element abundance patterns. For normalizing values and sequence of elements, see Sun and McDonough (1989).

3.3. Leucogranite

The leucogranite plots in the granite field on total $K_2O + Na_2O$ vs. SiO_2 (TAS) diagram (Figure 3.1), and displays a wide range of potassium and sodium contents from medium- to high-K calc-alkaline series (K_2O = 1.94 – 4.08 wt%; Na_2O =3.27 – 5.41 wt%) (Figure 3.2; Table 3.1). Likewise, P_2O_5 contents varies to a large extent (0.05 to 0.20 wt%). However, the other major oxides shows a much narrow variation (SiO_2 = 74.22 – 76.80 wt%, Al_2O_3 = 13.82 – 15.02 wt%, FeO* = 0.27 – 1.54 wt%, MgO = 0.04 – 0.08 wt%). Large variations in K_2O and Na_2O contents can be explained by large variation of grain size from normal granitic to pegmatitic domains, and our inability to take very large representative sample. The aluminum saturation index (ASI) ranges from 1.16 to 1.35, suggestive of peraluminous affinity. Mg number ranges from 7.7 to 22.9. This is in line with the highly evolved nature of the leucogranites. The peraluminous nature is compatible with the local presence of muscovite and garnet. Major and trace elements shows clustering in the Harker diagrams, apart from large variations in K_2O, Na_2O and P_2O_5 abundances at the nearly identical silica contents (Figure 3.2; 3.5).

$REE_{(cn)}$ patterns of the leucogranite samples can be divided to 2 types.

(i) Type-I: The samples 37b, 110b, 140, 142, and 219 are generally characterized by concave-upward shape. [$(La / Yb)_{cn}$ = 0.67 – 3.69] with pronounced negative Eu anomaly (Eu / Eu* = 0.14 – 0.65) (Figure 3.13). Form this we can infer that the source of this type of rocks is plagioclase bearing, and garnet-free despite the presence of igneous garnet in the rock. In addition, this profile may indicate fractionation of phosphate minerals such as apatite $(Ca_5PO_4)_3(F, Cl, OH)$ and xenotime (YPO_4).

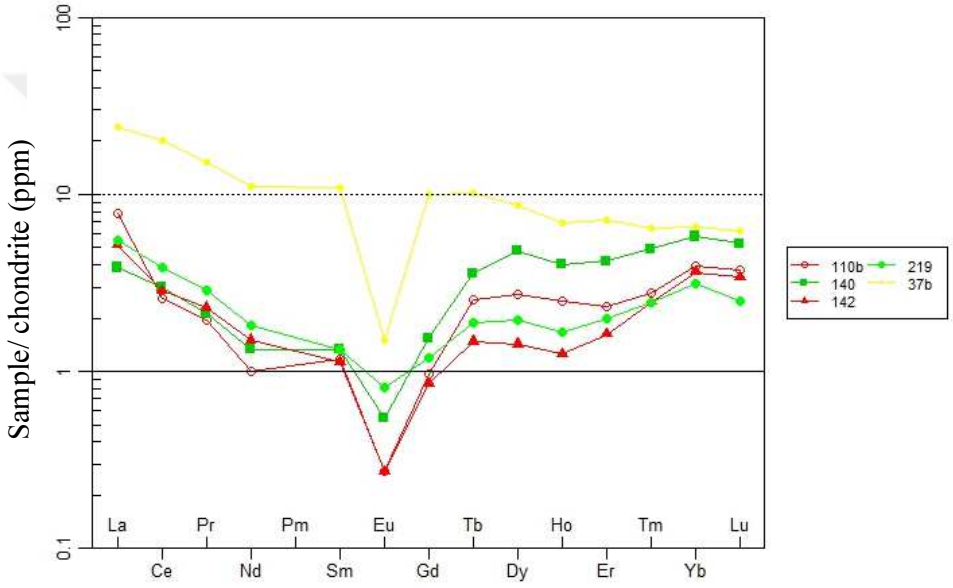

Figure 3.13: Type-I leucogranite samples. Chondrite-normalized rare earth element diagram. Normalizing values were taken from Boynton (1984).

(ii) Type-II: The samples 141 and 211 characterized by pronounced concave-upward shape whereby the light rare earth elements are hardly fractionated relative to the heavy ones [$(La/Yb)_{cn}$ = 1.69 – 2.84]. The Eu do not show any marked anomaly (Eu / Eu* = 0.94 - 1.03) (Figure 3.14).

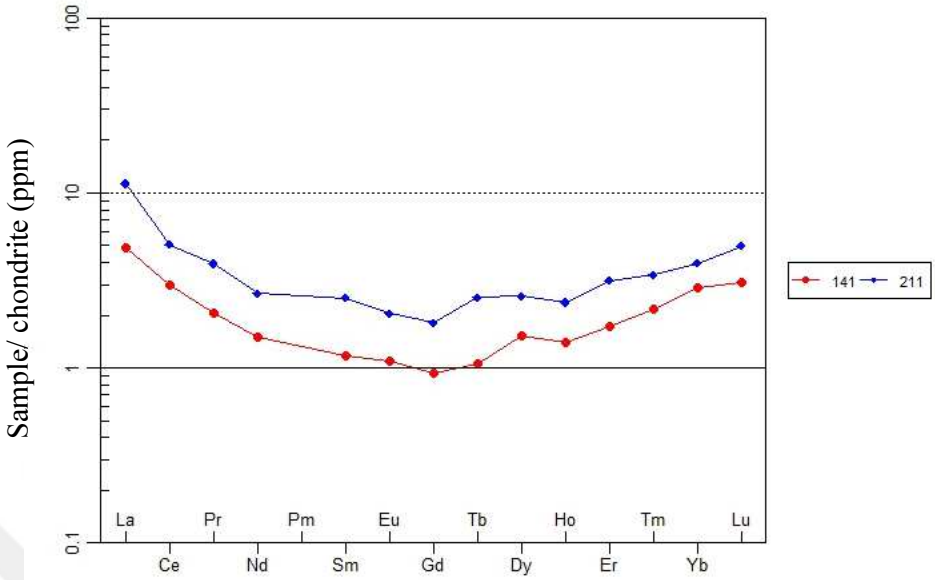

Figure 3.14: Type-II leucogranite samples. Chondrite-normalized rare earth element diagrams. Normalizing values were taken from Boynton (1984).

On $MEVD_{(pmn)}$, (i) the samples 37b, 110b, 140, 142, and 219 are generally display marked negative anomalies in Ba, Th, Nb, La, Ce, Pr, Sr Nd and extreme anomaly in Ti (Figure 3.15) which indicates fractionation in sphene. Generally the melt is depleted in HFSEs. However these samples have positive anomalies in some of the LILEs for example Cs, Rb and K, and also some of HFSEs such as U, P and Zr (Figure 3.15).

Enrichment in LILEs indicates crustal source of magma, because of the fact that LILEs are concentrated in the continental crust (Pearce et al 2005). (ii) The samples 141 and 211 have similar profile with smaller positive Zr anomaly in sample 211 (Figure 3.16).

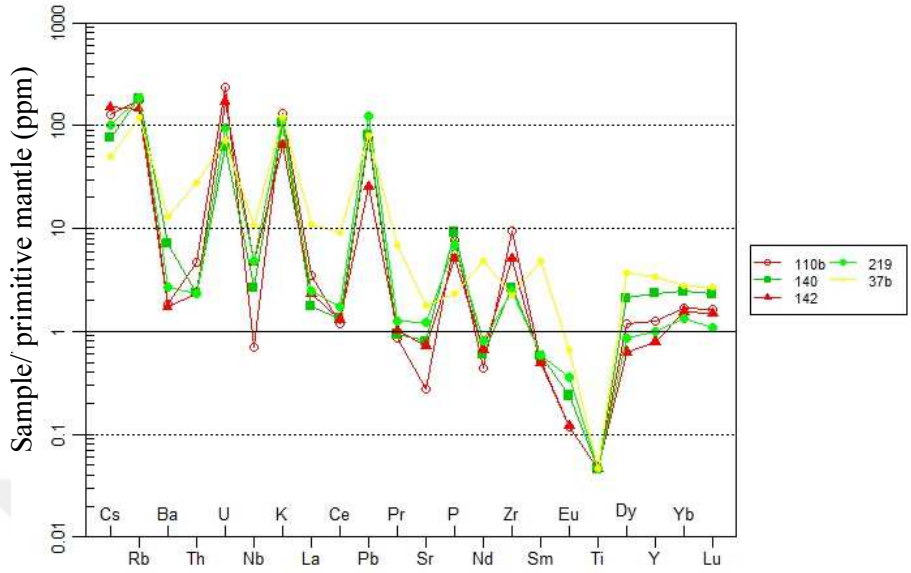

Figure 3.15: Type-I leucogranite samples. Primitive mantle-normalized element abundance patterns. For normalizing values and sequence of elements, see Sun and McDonough (1989).

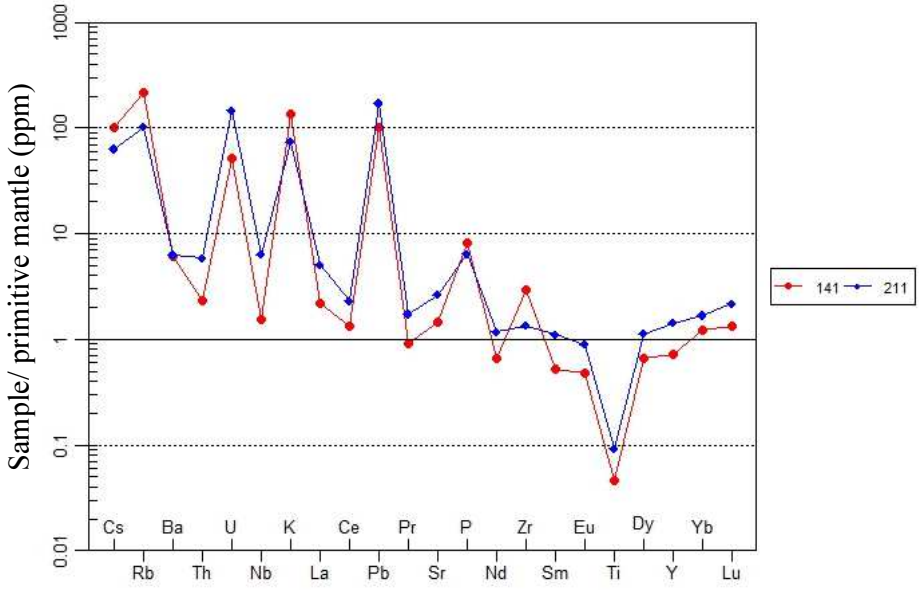

Figure 3.16: Type-II leucogranite samples. Primitive mantle-normalized element abundance patterns. For normalizing values and sequence of elements, see Sun and McDonough (1989).

3.4. Muscovite-biotite Granite

The muscovite-biotite granite shows a narrow compositional variation (SiO_2 = 71.28 – 73.24 wt%, Al_2O_3 = 14.74 – 15.34 wt%, FeO* = 1.26 – 1.90 wt%, MgO = 0.27 – 0.78 wt%, Na_2O = 2.84 – 3.10 wt%, K_2O = 5.15 – 6.22 wt% (Table 3.2). This type of

rock is also characterized by high values of potassium relative to CaO and Na_2O (Table 3.2). The two-mica granite plots in the granite field on total $K_2O + Na_2O$ vs. SiO_2 diagram (Figure 3.1). The ASI ranges from 1.17 to 1.26. Furthermore Mg number ranges from 25.58 to 39.72. Similar to leucogranite, presence of strongly aluminum rich minerals such as muscovite and biotite is compatible with the peraluminous feature. The muscovite-biotite granite plot on divide between the high-K calcalcaline and shoshonitic series on the SiO_2 vs. K_2O diagram after Peccerillo and Taylor (1976), thus representing the most K-rich intrusive rock type in the Sarıcakaya complex (Figure 3.2).

$REE_{(cn)}$ patterns of the muscovite-biotite granite (Figure 3.17) are characterized by extreme depletion of the HREEs relative to the LREEs $(La/Yb)_{cn}$ ranges form 36.12 – 45.68. This is most likely to indicate the presence of garnet in the source. The samples show pronounced negative Eu anomaly (Eu/Eu* = 0.4 – 0.5) indicating fractionation of plagioclase. (Table 3.2; Figure 3.17).

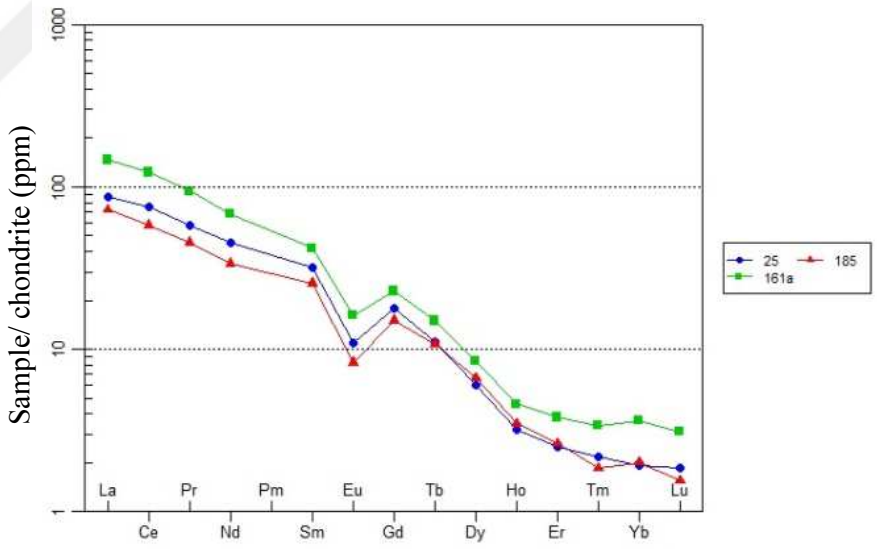

Figure 3.17: Muscovite-biotite granite samples. Chondrite-normalized rare earth element diagrams. Normalizing values were taken from Boynton (1984).

On $MEVD_{(pmn)}$, the muscovite-biotite granite is generally characterized by enrichment in LILEs such as Cs, Rb and K which may indicate partial melting of meta-pelite. However HFSEs like U, Nd, Sm and Dy also marked by positive anomalies (Figure 3.18). On the other hand depleted in Ba, Nb, Sr, Zr and Ti. The extreme depletion in Ti could be controlled by fractionation of rutile, sphene and ilmenite (Figure 3.18).

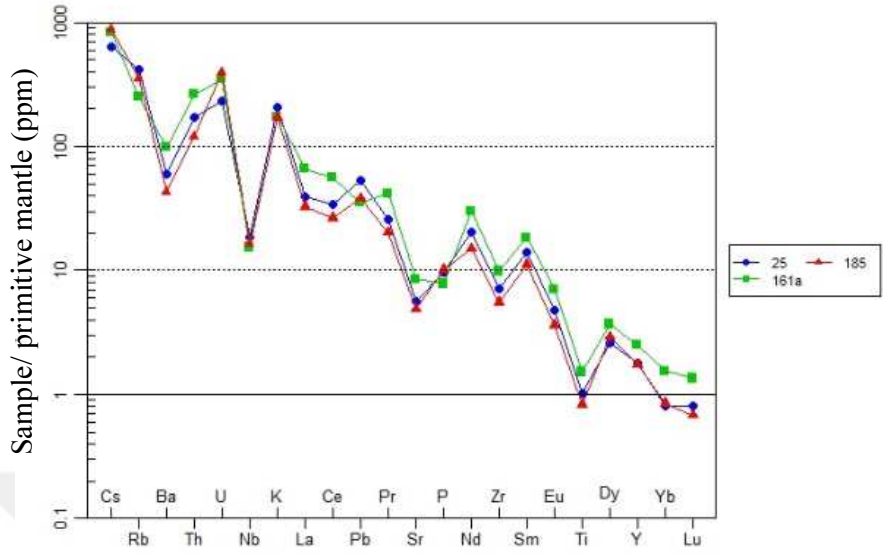

Figure 3.18: Muscovite-biotite granite samples. Primitive mantle-normalized element abundance patterns. For normalizing values and sequence of elements, see Sun and McDonough (1989).

3.5. Cumulate Gabbro

$REE_{(cn)}$ patterns of the cumulate gabbro (Samples 116a, 169 and 179) (Figure 3.19) are characterized by positive Eu anomaly (Eu/Eu* = 1.31 – 2.83). This indicates accumulation of plagioclase. The depletion of the HREEs relative to the LREEs $(La/Yb)_{cn}$ ranges form (2.82 – 4.49) probably indicates fractionation of garnet and hornblend (Figure 3.19). Sample 167 has similar REE profile with higher values of these elements and less pronounced positive Eu anomaly (Figure 3.19).

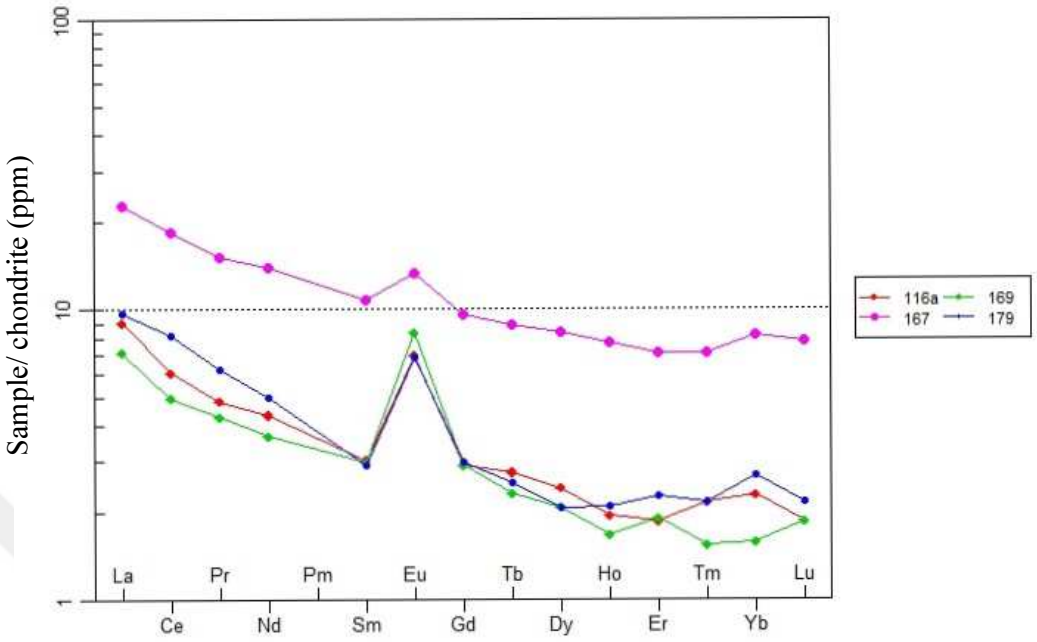

Figure 3.19: Cumulate gabbro. Chondrite-normalized rare earth element diagrams. Normalizing values were taken from Boynton (1984).

4. TECTONIC SETTING

4.1. Granite Tectonic Discrimination

The quartz diorite, hornblende-biotite granite and leucogranite plotted in the field of magmatic-arc granite of Pearce et al (1984) diagram (Figure 4.1). The two mica granite falls in syn-collisional granites region (Figure 4.1). This is based on the abundances of rare earth elements (Rb, Nb Y, Tb and Ta) in the rocks.

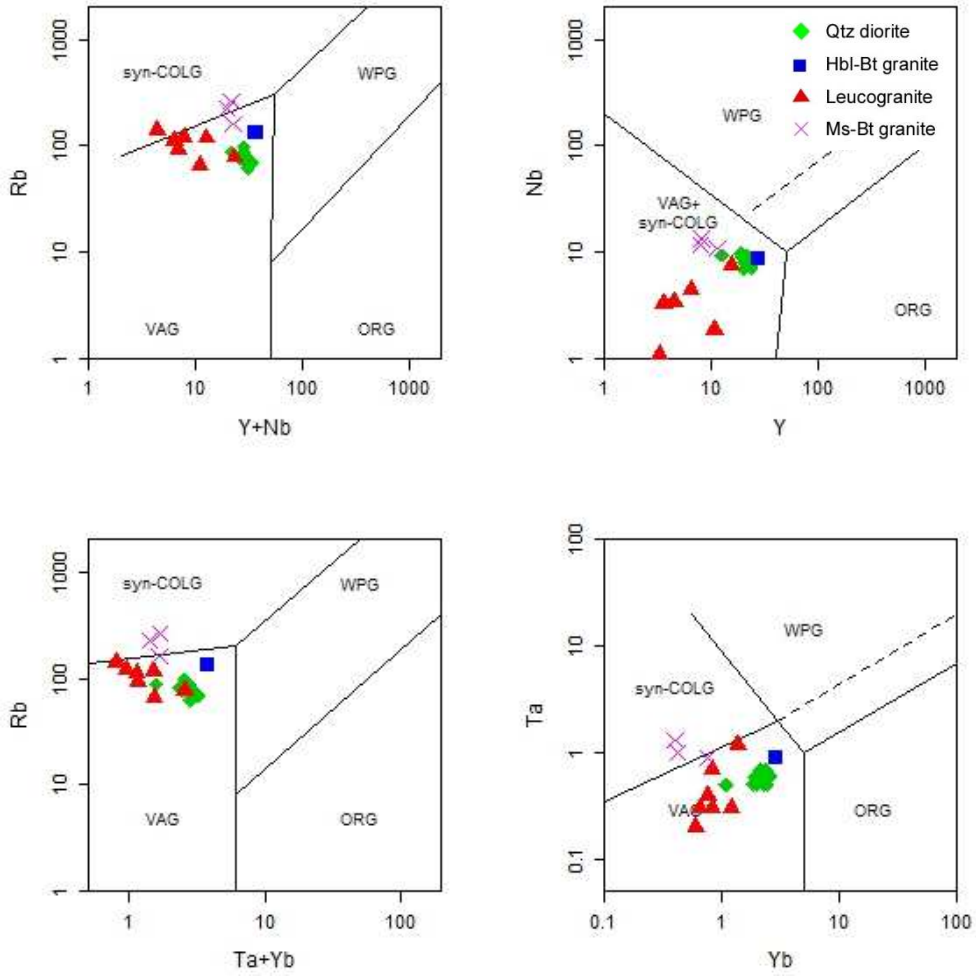

Figure 4.1: Locations of the different type of the Sarıcakaya intrusive rocks on tectonic discrimination diagram of Pearce et al. (1984). Syn-COLG: Syn-collision granite; WPG: Within plate granite; ORG: Ocean ridge granite; VAG: Volcanic arc granite.

4.2. Tectonic Explanation

The Carboniferous magmatism of Sarıcakaya complex can be explained as result of subduction (Okay and Topuz, 2016). This south dipping subduction of the Rheno-Hercynian oceanic plate between the northern continental domain (Istanbul zone) and Sakarya Zone forming magmatic arc (Okay and Topuz, 2016) (Figure 4.2). The southern margin of Sakarya acted as a passive margin (Okay and Topuz, 2016).

During Permian, the passive Laurasia margin converted to an active margin with the Paleo-Tethys oceanic plate dipping north under Laurussia (Okay and Topuz, 2016) (Figure 4.2). On the other hand, Candan et al (2016) suggest dual subduction both under Laurasia (northward) and southward subduction under Gondwana for the Paleo-Tethys oceanic plate between Early Carboniferous and Late Permian.

The quartz diorite most likely to be formed in the magmatic arc setting. In contrast the two mica granites are possibly formed in syn-collisional setting due to partial melting of continental crust. The melting of the crust can be explained by shortening in the Variscan orogeny (The collision between Sakarya zone and Laurasia margin) resulted possibly in crustal thickening and uplift which cause melting of the thick crust (Okay and Topuz, 2016).

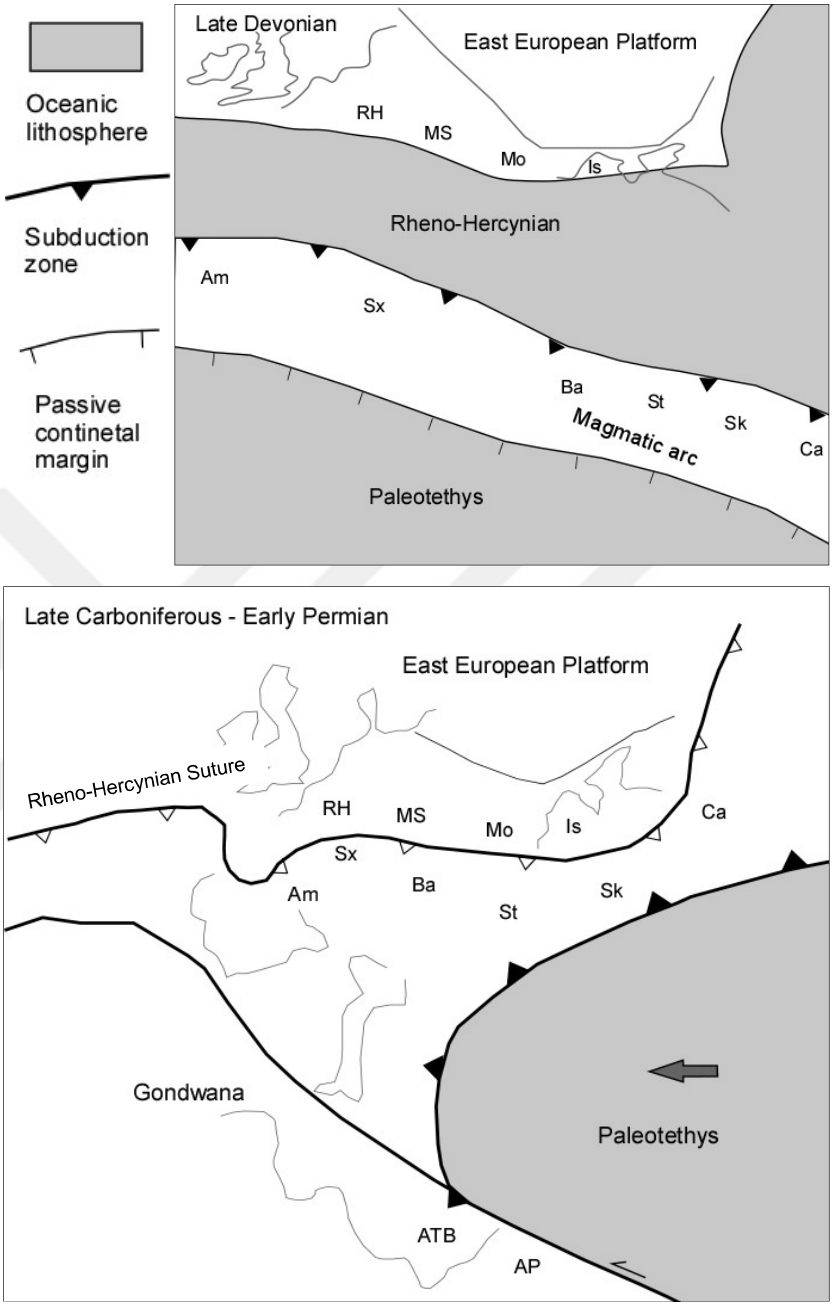

Figure 4.2: Paleogeographic maps showing a possible model for the Variscan evolution (modified after Okay and Topuz, 2016). Am: Armorica, AP: Arabian Platform, ATB: Anatolide–Tauride Block, Ba: Balkanides, Ca: Caucasus, MS: Moravia–Silesia, RH: Rheno-Hercynian, Sk: Sakarya, St: Strandja, Sx: Saxo-Thuringian.

5. CONCLUSIONS AND RECOMMENDATION

The principal conclusions of this study are as follows:

1. The metamorphic rocks are migmatitic gneiss, amphibolite, micaschist, in addition to metagranite and metagabbro. The most abundant metamorphic rocks are gneiss and amphibolite. This rock assemblage represents continental sedimentary and igneous protolith, however there is no signs of oceanic domain protolith. The rocks were subjected to amphibolite-facies metamorphism above muscovite + quartz stability.
2. The Sarıcakaya complex is amphibolite facies metamorphic rocks (probably carboniferous) intruded by distinctive types of intrusive. The intrusive includes quartz diorite, hornblende-biotite granite, leucogranite and muscovite-biotite granite, besides cumulate peridotite and gabbro. The dominant intrusive rocks are quartz diorite and hornblende-biotite granite (10-20 km long, 2-3 km across), whereas leucogranite, two-mica granite and cumulate rocks are limited to voluminously minor (50-800 m long and 1-50 m across) within the complex.
3. Geochemical data indicates that the quartz diorite is medium- to high-potassium calcalkaline. It is metaluminous and I-type granitic rock with mafic microgranular enclaves characteristic for magma mixing of differentiated mantle and crustal melts. The hornblende-biotite granite is high-potassium calcalkaline, peraluminous (ASI=1.13) and I-type granite.
4. The leucogranite are medium- to high-potassium calcalkaline. On the other hand, the two mica granite is high-potassium calcalkaline to shoshonite rock. They are both peraluminous and S-type granite probably formed due partial melting of continental crust.
5. The granitic rocks of Sarıcakaya formed in orogenic setting either during active subduction or in a post-collisional setting during Carboniferous time. This subduction is tentatively related to the consumption of the oceanic domain between the northern continental domain (Istanbul zone) and Sakarya Zone with a south-

vergent subduction. There is no indication of subduction under the Sakarya Zone from the southern Paleo-Tethys during early to middle Carboniferous.

6. Since this study is performed with limited data, for better evaluation, more data should be acquired. The further work can include geochronological data, analyzing more samples from the hornblende-biotite granite and determining Sr-Nd-Pb isotopic characteristics of granitic rocks.

REFERENCES

Aysal, N., Ustaömer, T., Öngen, S., Keskin, M., Köksal, S., Peytcheva, I., and Fanning, M. (2012). Origin of the Early-Middle Devonian magmatism in the Sakarya Zone, NW Turkey: geochronology, geochemistry and isotope systematics. *Journal of Asian Earth Sciences* 45, 201–222.

Bonin, B. (1988). Orogenic to non-orogenic magmatic events: overview of the late varsican magmatic evolution of the Alpine belt. *Turkish Journal of Earth Sciences* 7, 133-43.

Bonin, B. (1988). From orogenic to non-orogenic environments: evidence from associated magmatic episode. *Schweizerische mineralogische und petrographische Mitteilungen* 68, 301-11.

Bonin, B., **Bébien**, J., Masson, P. (2002). Granite: A planetary point of view. *Gondwana Research* 5, 261-273.

Bonin, B., Bébien, J. (2005). The granite-upper mantle connection in terrestrial planetary bodies: an anomaly to the current granite paradigm. *Lithos* 80: 131–145

Bonin, B. (2007). A-type granites and related rocks: Evolution of a concept, problems and prospects. *Litho* 97, 1-29.

Boynton, W.V. (1984). Geochemistry of the rare earth elements: meteorite studies. In: Henderson, P. (ed), Rare Earth Element Geochemistry, *Elsevier,* 63–114.

Candan, O., Akal, C., Koralay, O.E., Okay, A.I., Oberhänsli, R., Prelević, D., Mertz-Kraus, R. (2016). Carboniferous granites on the northern margin of Gondwana, Anatolide-Tauride Block, Turkey –Evidence for southward subduction of Paleotethys. *Tectonophysics.*

Delaloye, M., and Bingöl, E. (2000). Granitoids from Western and Northwestern Anatolia: Geochemistry and modeling of geodynamic evolution. *International Geology Review*, 42 3, 241-268.

Dokuz, A. (2011). A slab detachment and delamination model for the generation of Carboniferous high potassium I-type magmatism in the Eastern Pontides, NE Turkey: The Köse composite pluton. *Gondwana Res*. 9 (4), 926-944.

Duru, M., Pehlİvan, Ş., Dönmez, M., Ilgar, A., and Akçay, A. E. (2007). 1/100.000 Ölçekli Türkiye Jeoloji Haritaları, Bandırma H18 Paft ası [Geological Map of the Bandırma-H18 Quadrangle 2007, 1:100,000 Scale]. MTA Genel Müdürlüğü, Jeoloji Etüdleri Dairesi.

Papak, I., Coşkun, A., Ebeper, N. (2002). General Directorate of Mineral Research and Exploration (MTA, 2003/4), 1:1,250,000 scaled geological map of Turkey. Retrieved November 3, 2016, from http://www.maps.mta.gov.tr.

Göncüoğlu, M. C., Dirik, K., and Kozlu, H. (1996). Pre-alpine and alpine terranes in Turkey: explanatory notes to the terrane map of Turkey. *Ann. Géol. des Pays Hél.*, 37: 515–536.

Göncüoğlu, M. C., Turhan, N., Şentürk, K., Özcan, A., Uysal, S., and Yalınz, M. K. (2000). A geotraverse across northwestern Turkey: tectonic units of the Central Sakarya region and their tectonic evolution. In: Bozkurt, E., Winchester, J.A. & Piper, J.D. (eds) Tectonics and Magmatism in Turkey and the Surrounding Area. *Geological Society, London, Special Publications* 173, 139–162.

Hansen, J., Skjerlie, K.P., Pedersen, R.B., and De La Rosa, J. (2002). Crustal melting in the lower parts of island arcs: an example from the Bremanger Granitoid Complex, west Norwegian Caledonides; Contributions to Mineralogy and Petrology, v. 143, p. 316-335.

Ilbeyli, N., Demirbilek M., and Kibici Y. (2015). Geochemistry and petrogenesis of the Late Paleozoic magmatism in the Sakarya Zone (NW Turkey). *Neues jahrbuch fur mineralogie-abhandlungen,* vol.192, pp.177-194.

Kadıoğlu, Y. K., Aydal, D., and Kayadibi, O. (1994). The investigation of Bilecik-Sögüt gold mineralization. *Bulletin of the GeologicaI Congress of Thrkey*, NO.9, 252-259. (In Turkish).

Ketin, T. (1966). Anadolu'nun tektonik birlikleri. M.T.A. Derg. No. 66, s. 20-34, Ankara.

Kibici, Y., Ilbeyli, N., Yıldız, A., and Bağcı, M. (2010). Geochemical constraints on the genesis of the Sarıcakaya intrusive rocks, Turkey: Late Paleozoic crustal melting in the central Sakarya Zone*. Chemie der Erde 70 (2010) 243–256.*

Okay, A. I. (2000). Was the Late Triassic orogeny in Turkey caused by the collision of an oceanic plateau? *Geological Society, London, Special Publications* 2000, v. 173, p. 25-41.

Okay, A. I. (2008). Geology of Turkey: A Synopsis. *Anschnitt,* 21, 19-42.

Okay, A. I., and Leven, E. J. (1996). Stratigraphy and paleontology of the Upper Paleozoic sequence in the Pulur (Bayburt) region, Eastern Pontides. *Turkish Journal of Earth Sciences,* 5: 145-155.

Okay, A. I. and Sahinturk, O., (1997). Geology of Eastern Pontides.

Okay, A. I., and Tüysüz, O. (1999). Tethyan sutures of northern Turkey, *Geological Society, London, Special Publications* 1999, v. 156, p. 475-515.

Okay, A. I., Monod, O., and Monie, P. (2002). Triassic blueschists and eclogites from northwest Turkey: vestiges of the Paleo-Tethyan subduction. *Lithos* 64, 155-178.

Okay, A. I., Satir, M., and Siebel, W. (2006). Pre-Alpide Palaeozoic and Mesozoic orogenic events in the Eastern Mediterranean region. *Geological Society, London, Memoirs,* 32, 389–405.

Okay, A. I., and Topuz, G. (2016). Variscan orogeny in the Black Sea region. Int J Earth Sci (Geol Rundsch). DOI 10.1007/s00531-016-1395-z

Peccerillo, A., and Taylor, S. R. (1976). Geochemistry of Eocene calc-alkaline volcanic rocks from the Kastamonu area, northern Turkey. Contrib. Mineral. Petrol. 58, 63–81.

Pearce, J. A., Harris, N. B. W., and Tindle, A., J. (1984). Trace element discrimination diagrams for the tectonic interpretation of granitic rocks. J. Petrol., 25, 956-83.

Pearce J. A., Stern R. J., Bloomer S. H., Fryer P. (2005). Geochemical mapping of the Mariana arc–basin system: implications for the nature and distribution of subduction components. *Geochemistry Geophysics Geosystems* 6: Q07006.

Sun, S., and McDonough, W. (1989). Chemical and isotopic systematics of oceanic basalts: implications for mantle composition and processes. *Geological Society, London, Special Publications* 1989, v. 42, p. 313-345.

Şengör, A. M. C., and Yilmaz, Y. (1981). Tethyan evolution of Turkey: a plate tectonic approach. *Tectonophysics,* 75 (1981) 181-241.

Topuz, G., Altherr, R., Satir, M., and Schwarz, W. H. (2004b). Low grade metamorphic rocks from the Pulur complex, NE Turkey: implications for pre-Liassic evolution of the Eastern Pontides. *International Journal of Earth Sciences* 93, 72–91.

Topuz, G., Altherr, R., Schwarz, W. H., Dokuz, A., and Meyer, H. (2007). Variscan amphibolitefacies metamorphic rocks from the Kurtoğlu metamorphic

complex (Gümüşhane area, Eastern Pontides, Turkey). *International Journal of Earth Sciences (Geol Rundsch)* 96, 861–873.

Topuz, G., Altherr, R., Siebel, W., Schwartz, W. H., Zack, T., Hasözbek, A., Barth, B., Satır, M., and Şen, C. (2010) Carboniferous high-potassium I-type granitoid magmatism in the Eastern Pontides: the Gümüşhane pluton (NE Turkey). Lithos 116:92–110.

Topuz, G., Okay, A. I., Altherr, R., Schwarz, W., Sunal, G., and Altinkaynak, L. (2014). Triassic warm subduction in northeast Turkey: Evidence from the Ağvanis metamorphic rocks. *Island Arc* (2014) 23, 181–205.

Ustaömer, T., and Robertson, A. H. F. (2010). Late Palaeozoic–Early Cenozoic tectonic development of the Eastern Pontides (Artvin area), Turkey: stages of closure of Tethys along the southern margin of Eurasia. *Geological Society, London, Special Publications* 340, 281–327.

Ustaömer, P. A., Ustaömer, T., and Robertson, A. H. F. (2012). Ion Probe U-Pb Dating of the Central Sakarya Basement: A peri-Gondwana Terrane Intruded by Late Lower Carboniferous Subduction/Collision-related Granitic Rocks. *Turkish Journal of Earth Sciences*. Vol. 21, 2012, pp. 905–932.

Wedepohl, K. H. (1991) Chemical composition and fractionation of the continental crust. *Geol. Rundsch.* 80, 207-223.

Yılmaz, Y. (1977). Bilecik-Söğüt Dolayındaki Eski Temel Karmaşığı'nın Petrojenetik Evrimi [Petrogenetic Evolution of the Old Basement Complex in the Bilecik-Söğüt Area]. Habilitation Thesis, İstanbul University [in Turkish with English abstract, unpublished].

CURRICULUM VITAE

Name Surname: Malik Othman

Place and Date of Birth: Alkhums city, Libya, 1976

E-Mail: malikotman@yahoo.com

EDUCATION:

- B.Sc.: 1998, El-Mergib University, Faculty of Arts and Sciences, Earth Sciences.
- M.Sc.: 2016, Istanbul Technical University, Eurasia Institute of Earth Sciences.

PROFESSIONAL EXPERIENCE

- 2001-2003 Demonstrative at El-Mergib University, Earth Sciences Department.
- 2005-2009 Petroleum geologist at Woodside Energy North Africa.
- 2010-2013 Petroleum geologist at Royal Dutch Shell.
- 2016 Completed Master at ISTANBUL Technical University.